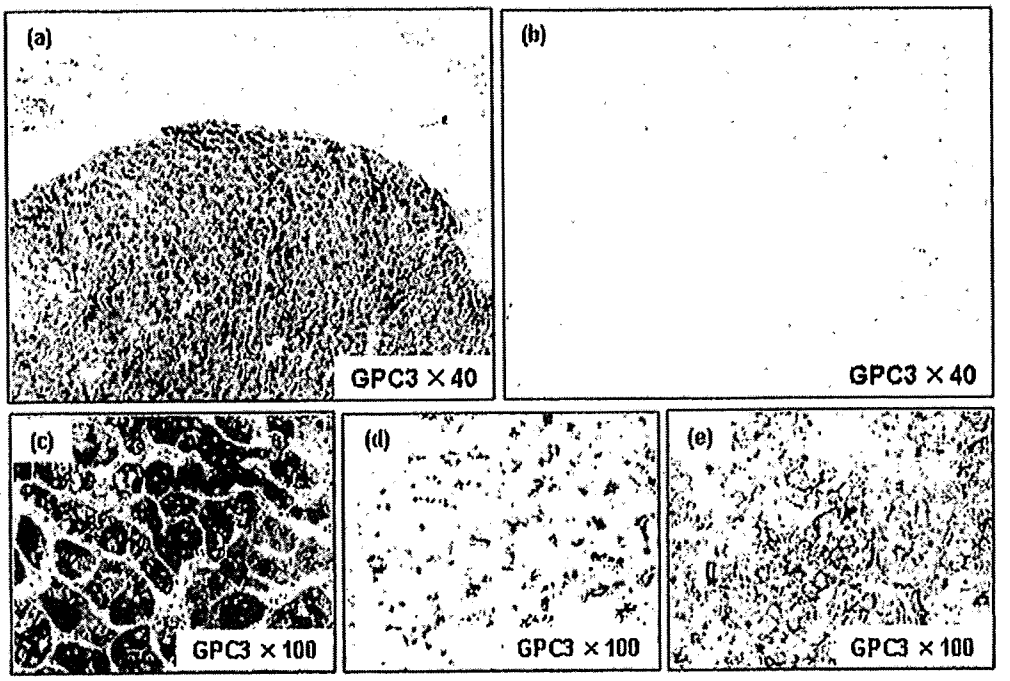

Figure 1. GPC3 expression was specific to HCC and absent in ICC. Immunohistochemical detection of GPC3 expression in HCC (a) and ICC (b) (magnification, x40). Immunostaining patterns of HCC: (c) diffuse in cytoplasm, gulanular in cytoplasm (d), and membranous (e).

Table I. Correlation of positive for GPC3 staining and tumor grade.

Grade of tumor	HCC					ICC		
		GPC3						
	No. of case	-	±	+	positivity	No. of case	GPC3 positivity	P-value
Well-differentiated	15	6	5	4	9 (60%)	8	0 (0%)	
Moderately differentiated	18	2	4	12	16 (89%)	10	0 (0%)	
Poorly differentiated	13	2	5	6	11 (85%)	10	0 (0%)	
Total	46				36 (78%)	28	0 (0%)	<0.0001

-, negative (<10%); ±, weakly positive (10-30%); +, positive (>30%).

differentiation level, GPC3 was expressed in 9 (60%) of 15 well differentiated, 16 (89%) of 18 moderately differentiated and in 11 (85%) of 13 poorly differentiated HCC (Table I). AFP was expressed in 3 (20%) of 15 well differentiated, 6 (33%) of 18 moderately differentiated and in 7 (54%) of 13 poorly differentiated HCC (data not shown). The expression level of GPC3 was lower in well differentiated HCC than in the other HCC grades, though the difference was not statistically significant (well- vs. moderately differentiated: P=0.054, well- vs. poorly differentiated: P=0.150). Thus, GPC3 expression is also a good indicator for malignancy levels.

GPC3 expression was observed specifically in pathological HCC component in CHC. There are discrepancies between preoperative diagnosis and pathological findings for CHC patients. Diagnostic results and the expression of tumor markers of 11 CHC patients are summarized in Table II. Initial diagnosis was carried out by H.E. staining. Among these 11 patients, 7 patients (63.6%) were diagnosed as HCC and 3 (27.3%) were ICC. Only 1 patient (9%) of the 11 CHC was correctly diagnosed as CHC. To seek the possibility to use GPC3 immunostaining to detect HCC component (cp) in CHC, combination of antibodies against GPC3, AFP, HepPar1, CK7 and CK17 were used. In addition to AFP, HepPar1 is frequently used as marker for HCC (4-8) and CK 7 and CK19 for ICC (9-11).

Among 11 CHC cases, 4 cases preoperatively diagnosed as HCC were chosen to represent the collision and transitional type of CHCs based on the macroscopic features

Table II. Correlation of immunostaining varieties and pathological components of CHC.

Pt. no.	Preoperative diagnosis	Macroscopic diagnosis	Pathological hepatocellular carcinoma component					Pathological cholangiocarcinoma component				
			GPC3	AFP	HepPar1	CK7	CK19	GPC3	AFP	HepPar1	CK7	CK19
1	HCC	CHC	+	+	-	+	+	-	-	-	-	-
2	HCC	HCC	+	-	-	-	-	-	-	+	+	+
3	HCC	HCC	+	-	+	-	-	±	-	-	+	+
4	CHC	HCC	+	+	+	-	-	±	-	-	+	+
5	HCC	CHC	+	-	+	-	-	-	-	-	+	+
6	HCC	CHC	+	-	-	-	-	-	-	+	+	+
7	ICC	CHC	±	-	-	±	+	-	-	-	+	+
8	HCC	HCC	+	+	-	-	-	-	+	-	+	+
	Total ±		8/8	3/8	3/8	3/8	2/8	2/8	1/8	2/8	7/8	7/8
	positive rate (%)		100	38	38	38	25	25	13	25	88	88
9	ICC	ICC	-	-	-	-	-	-	-	-	+	+
10	HCC	ICC	-	-	-	+	±	-	-	-	+	+
11	ICC	ICC	-	-	-	+	+	-	-	-	+	+
	Total ±		0/3	0/3	0/3	2/3	2/3	0/3	0/3	0/3	3/3	3/3
	positive rate (%)		0	0	0	67	67	0	0	0	100	100

-, negative (<10%); ±, weakly positive (10-30%); +, positive (>30%); HCC, hepatocellular carcinoma; ICC, intrahepatic cholangiocarcinoma; CHC, combined hepatocellular and cholangiocarcinoma; GPC3, glypican-3; AFP, α-fetoprotein; HepPar1, hepatocyto-paraffin 1; CK, cytokeratin; CC, cholangiocarcinoma.

in cut surface. In Fig. 2, macroscopic observation and the immunostained histological sections are shown. These sections include 2 elements with pathological HCC cp forming bile production and trabecular growth pattern by eosinophilic staining and cholangiocarcinoma (CC) cp forming mucin production or gland formation by basophilic staining. Cases 1-8 were GPC3 positive, and cases 9-11 were negative for GPC3 in the HCC cp. Macroscopic, histological and immunohistochemical features of cases 2, 6, 8 and 10 are shown in Fig. 2a, b, c and d. Case 2 had greenish white and yellow nodules within the same tumor mass in the cut surface. HCC subtypes such as simple nodular and confluent multinodular type exist. Case 2 exhibited the features of HCC with multinodular type (Fig. 2a-i). Pathological diagnosis by H.E. staining revealed CHC pathologically (Fig. 2a-ii and -iii), which was so-called 'collision'-type tumor as reported by Goodman *et al* (30). A 'collision'-type tumor is coincidental occurrence of HCC and CC within the same tumor mass (31). GPC3 was positive (Fig. 2a-iv), but AFP and HepPar1 were not detected in HCC cp (Fig. 2a-v and -vi). Although HepPar1 is generally used as HCC marker, it was unexpectedly stained in CC region as well as CK7 and CK19 (Fig. 2a-vii and -viii).

Case 6 showed pale and lobulated phenotype in the cut surface macroscopically (Fig. 2b-i), and pathological diagnosis was also confirmed by H.E. staining (Fig. 2b-ii and -iii). This was so-called 'transitional' type tumor (30). A 'transitional' type tumor has an area of HCC that appears to transform into CC (31). GPC3 was stained in pathological HCC cp (Fig. 2b-iv) where AFP was negative (Fig. 2b-v). The HCC region was surrounded by pathological CC cp with the staining for CK7 (Fig. 2b-vii). HepPar1 and CK19 were detected in the same region with CC cp (Fig. 2b-vi and -viii). HepPar1 stained the CC cp as in case 2. The immunoreactivity of CK19 was not consistent with that of CK7.

Case 8 was diagnosed as HCC similarly to cases 2 and 6, but mixed tumor masses with white and gray in the cut surface were observed (Fig. 2c-i and c-ii). Both GPC3 and AFP were positive in HCC cp (Fig. 2c-iv and -v). HepPar1 was stained in CC cp (Fig. 2c-vi). CK7 and CK19 were positive in CC cp (Fig. 2c-vii and -viii), especially CK19 was more specific for CC cp than CK7. These three cases (cases 2, 6 and 8) indicated that detecting GPC3 can compensate for AFP and enhance the ability to identify the presence of HCC cp in CHC.

Cases 9, 10 and 11 were negative for GPC3 expression in several tumors. Macroscopically, they had the features of ICC with irregular shaped, white solid tumor masses. As an example, case 10 is shown in Fig. 2d. Althogh case 10 was diagnosed as HCC preoperativerly, it showed macroscopic freatures of ICC with the presence of abundant fibrous stroma and indistinct tumor margin (Fig. 2d-i). This case was later diagnosed as CHC based on the pathological examination (Fig. 2d-ii and d-iii). GPC3, AFP and HepPar1 were not detected in either HCC cp or CC cp (Fig. 2d-iv, -v, and -vi). CK7 was stained diffusely in the tumor (Fig. 2d-vii), and CK19 expression was more specific in CC cp than CK7 (Fig. 2d-viii). These 3 cases showed positive staining

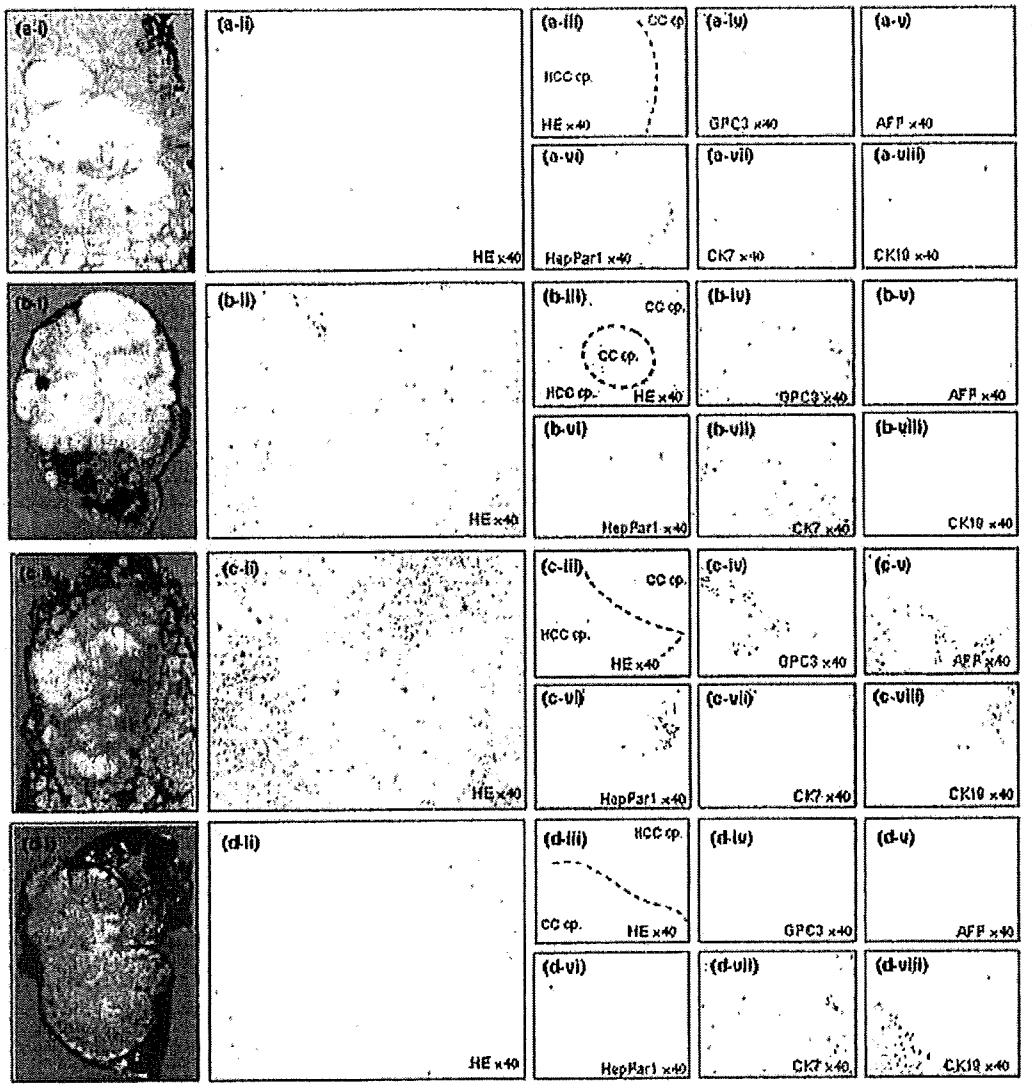

Figure 2. Macroscopic, histological and immunohistochemical features of four cases of CHC (a, case 2; b, case 6; c, case 8; d, case 10 in Table II. (a-i) Macroscopic feature in cut surface of case 2 tumor. (a-ii) The histological structure can be also devided into 2 types. HCC component showed expansive growth oppressing the cholangiocarcinoma component. (a-iii) Collision border between hepatocellular carcinoma and cholangiocarcinoma component are indicated as dots. The tumor cells within mainly hepatocellular carcinoma component showed only expression of GPC3 (a-iv) without expression of AFP (a-v). In the opposite side, the glandular area with cholangiocarcinoma component shows HepPar1 (a-vi), CK7 (a-vii) and CK19 expression (a-viii). (b-i) Case 6 shows macroscopic CHC feature in tumor cut surface that was suspected out HCC preoperatively. (b-ii) The histological cholangiocarcinoma component forming trabeculae with columnar appearance was surrounded by HCC component forming hepatoid structure. (b-iii) A dotted line is a boundary of HCC in the H.E. staining. The tumor cells within transitional region were positive for GPC3 (b-iv), CK 7 (b-vii) and CK 19 (b-viii). The difference was recognized between hepatocellular carcinoma component and cholangiocarcinoma component because GPC3 positive area encircled the CK7 area. The expressions of AFP (b-v) and HepPar1 (b-vi) were not observed. (c-i) Though case 8 was also suspected to be HCC preoperatively, the macroscopic features showed atypical HCC with mixed white and gray and indistinct tumor border. (c-ii) The cholangiocarcinoma component was obviously composed of structural gland formation. (c-iii) Collision area was distinguished histopathologically by a dotted line. The tumor cells of HCC component showed not only GPC3 (c-iv) but also AFP expression (c-v). In the glandular area of cholangiocarcinoma component, HepPar1 was expressed (c-vi), but CK7 not at all (c-vii) and CK19 shows weak positive expression (c-viii). (d-i) Case 10 shows macroscopic ICC features in tumor cut surface that was suspected as HCC preoperatively. (d-ii) The histological structure can be devided into 2 types with cholangiocarcinoma component forming trabeculae with columnar appearance and HCC component forming hepatocellular structures. (d-iii) A dotted line is a boundary of HCC in the H.E. GPC3 (d-iv), AFP (d-v) and HepPar1 (d-vi) were not stained, but CK7 (d-vii) and CK19 (d-viii) stained the cholagiocarcinoma component.

for CK7 and CK19 in CC ep, but not AFP or HepPar1 in HCC ep. Therefore, accuracy of CHC diagnosis can be achieved by combination of multiple tumor markers in addition to morphological characteristics: GPC3 that is specific for pathological HCC ep of CHC, and CK7 and CK19 that are specific for pathological CC ep of CHC.

Discussion

The diagnosis for HCC, ICC and CHC has been routinely performed by histopathological examination. Additionally, diagnosis of HCC is done by supplementary immunohistochemical analysis for AFP and HepPar1. Until now, though

the sensitivity is limited, AFP has been regarded as the most useful marker for HCC (4,32-34). HepPar1 is also widely used for HCC to distinguish between primary HCC and ICC. However, both markers are limited for the ability to discriminate different levels of malignancy in HCC because its sensitivity drops substantially in poorly differentiated HCC, and it does not discriminate between benign and malignant liver cancers (35). As these biomarkers frequently results in misdiagnosis, in this study, we showed that GPC3 is more sensitive to detect HCC compared to AFP. Due to the fact that GPC3 was downregulated in ICC (36), GPC3 may help to separate HCC from ICC.

CHC is the least common primary cancer of the liver but followed by an aggressive growth, it tends to metastasize to many organs leading to significantly poorer prognosis than HCC and ICC (31,37,38). Correct diagnosis leads to both appropriate treatment and better outcome for the patients. Nishie, *et al* reported that one third (nine of 27 cases) of patients with CHC were correctly diagnosed by enhanced computed tomography (39). In our study, only one of the 11 (9.1%) patients with CHC was correctly diagnosed before operation without fine needle aspiration biopsy. The difficulty to pathologically distinguish CHC from HCC and ICC comes from glandular or pseudoglandular structures in HCC and solid or trabecular patterns in CC (37,38). We believe that combination with histopathological examination with GPC3 immunostaining and radiological examination can bring an accurate diagnosis and improved clinical therapies for the patients leading to a better prognosis.

We showed that the immunostaining for GPC3 is specific for HCC patients and not detected in ICC patients. This confirmed that detecting GPC3 may improve the method to diagnose CHC. Of the 11 cases of CHC, 8 displayed GPC3 expression in restricted area of HCC cp. We demonstarated that immunohistochemical staining of GPC3 in liver tumor helps to recognize the pathological HCC cp more precisely. GPC3 expression was observed with high frequency in the HCC cp compared with AFP and HepPar1. HepPar1 was unexpectedly stained in CC cp, but this has been observed previously as well (7,40). This could be due to a transition from HCC to ICC where HepPar1 is one of the molecules that is downregulated at later stages in the process. CK7 and CK19 have been already reported as good markers of biliary epithelial differentiation (41). These were highly expressed in pathological CC cp (10/11, 91%) in CHC. The positive immunoreactivity of CK19 was more distinct than that of CK7 whose staining was weaker. Our immunohistochemical data disclosed that GPC3 can be a better marker specific for HCC leading to a better confirmation for HCC component of CHC as well as for HCC. Moreover, it provided evidence of the biologic behavior of such combined tumors, which are phenotypically and genetically leaning toward either ICC with predominant biliary differentiation or HCC with hepatocellular differentiation (42,43).

Employing multiple tumor markers may also allow the accurate diagnosis of CHC containing both hepatocellular and biliary differentiation. Concerning sensitivity and specificity, the combination of GPC3 for HCC cp and CK19 for ICC cp seems to be useful in the diagnosis of liver cancer. For CHC, GPC3 positive/CK19 negative profile suggests HCC, GPC3 positive/CK19 positive indicates CHC, and GPC3 negative/CK19 positive essentially rules out HCC and suggests the possibility of CC or CHC.

We developed a new anti-cancer immunotherapy with GPC3 as a target (44-47), and the phase I clinical trial of GPC3-derived peptide vaccination for advanced HCC is now on going. Because this new immunotherapy is not indicated for ICC, immunohistochemical staining of GPC3 is a useful method to select eligible patients. Furthermore, if CHC would be justified as a target of our immunotherapy in future, immunohistochemical analysis for GPC3 expression is indispensable for the process of patient selection.

GPC3 is expressed in the group of cells that are AFP-positive and/or CK7/19-positive in injured livers with activation of oval cell compartment; an indication for liver repair and regeneration (48). In addition, CK7, CK19 and AFP are frequently expressed in biliary epithelial cells (49,50) and in immature fetal hepatoblasts (51,52). Liver progenitor cells originate from the canal of Hering, lined by both hepatocytes and biliary ductular epithelial cells (53). It is not clear whether GPC3 is expressed in hepatic embryonic progenitor cells or cancer stem cells, but GPC3 may be a marker for hepatic progenitor/stem cells. In CHC cases of 2, 3 and 4, GPC3, CK7 and CK19 coincided in the regions of HCC and CC. Although HCC and ICC are two different kinds of primary liver malignancies arising from different cell types as hepatocytes and cholangiocytes, co-localization of GPC3 and CK7/19 suggest that the CHC is originated from progenitor or oval cell. In addition, case 6 showed an HCC lesion with GPC3 positive immunostaining surrounded by CC (Fig. 2b). This finding suggests that GPC3-positive HCC tumor cells are derived from GPC3-negative CC mass. Moreover, we predict from the fact that GPC3 is expressed in embryonic liver and downregulated after birth in normal liver but reappears in cancer is due to its regulatory role in proliferative and dedifferentiated cells, like cancer cells that acquired a progenitor- or cancer stem cell-like characteristics.

In summary, we confirmed that GPC3 is a marker sensitive and specific for HCC, but not ICC. Moreover, we revealed that GPC3 was expressed specifically in the HCC cp in the CHC. Therefore, GPC3 is a molecule that is significant not only in clinical but also biological field. It is clinically an important biomarker that can be used for accurate diagnosis leading to a better treatment and prognosis. Also, biologically, it may be an indicator for the identity and the origin of the cancer cells.

Acknowledgments

This study was supported in part by Health and Labor Sciences Research Grants for Research on Hepatitis from the Ministry of Health, Labor, and Welfare, Japan, and a grant-in-aid for the Third-Term Comprehensive 10-Year Strategy for Cancer Control from the Ministry of Health, Labour and Welfare, Japan. Foundation for Promotion of Cancer Research in Japan, Japan Research Foundation for Clinical Pharmacology and Research Resident Fellowship from the Foundation for Promotion of Cancer Research, Japan (H.S.). We thank Dr Chinatsu Kojima (Section for Cancer Immunotherapy, Investigative Treatment Division,

Research Center for Innovative Oncology, National Cancer Center Hospital East) for technical assistance.

References

1. Aoki K, Takayasu K, Kawano T, *et al*: Combined hepatocellular carcinoma and cholangiocarcinoma: clinical features and computed tomographic findings. Hepatology 18: 1090-1095, 1993.
2. Ng IO, Shek TW and Nicholls J and Ma LT: Combined hepatocellular-cholangiocarcinoma: a clinicopathological study. J Gastroenterol Hepatol 13: 34-40, 1998.
3. Liu CL, Fan ST, Lo CM, *et al*: Hepatic resection for combined hepatocellular and cholangiocarcinoma. Arch Surg 138: 86-90, 2003.
4. Brumm C, Schulze C, Charels K, Morohoshi T and Kloppel G: The significance of alpha-fetoprotein and other tumour markers in differential immunocytochemistry of primary liver tumours. Histopathology 14: 503-513, 1989.
5. Wennerberg AE, Nalesnik MA and Coleman WB: Hepatocyte paraffin 1: a monoclonal antibody that reacts with hepatocytes and can be used for differential diagnosis of hepatic tumors. Am J Pathol 143: 1050-1054, 1993.
6. Minervini MI, Demetris AJ, Lee RG, Carr BI, Madariaga J and Nalesnik MA: Utilization of hepatocyte-specific antibody in the immunocytochemical evaluation of liver tumors. Mod Pathol 10: 686-692, 1997.
7. Leong AS, Sormunen RT, Tsui WM and Liew CT: Hep Par 1 and selected antibodies in the immunohistological distinction of hepatocellular carcinoma from cholangiocarcinoma, combined tumours and metastatic carcinoma. Histopathology 33: 318-324, 1998.
8. Lau SK, Prakash S, Geller SA and Alsabeh R: Comparative immunohistochemical profile of hepatocellular carcinoma, cholangiocarcinoma, and metastatic adenocarcinoma. Human Pathol 33: 1175-1181, 2002.
9. Maeda T, Kajiyama K, Adachi E, Takenaka K, Sugimachi K and Tsuneyoshi M: The expression of cytokeratins 7, 19, and 20 in primary and metastatic carcinomas of the liver. Mod Pathol 9: 901-909, 1996.
10. Sasaki A, Kawano K, Aramaki M, Nakashima K, Yoshida T and Kitano S: Immunohistochemical expression of cytokeratins in intrahepatic cholangiocarcinoma and metastatic adenocarcinoma of the liver. J Surg Oncol 70: 103-108, 1999.
11. Shimonishi T, Miyazaki K and Nakanuma Y: Cytokeratin profile relates to histological subtypes and intrahepatic location of intrahepatic cholangiocarcinoma and primary sites of metastatic adenocarcinoma of liver. Histopathology 37: 55-63, 2000.
12. Capurro M, Wanless IR, Sherman M, *et al*: Glypican-3: a novel serum and histochemical marker for hepatocellular carcinoma. Gastroenterology 125: 89-97, 2003.
13. Nakatsura T, Yoshitake Y, Senju S, *et al*: Glypican-3, overexpressed specifically in human hepatocellular carcinoma, is a novel tumor marker. Biochem Biophys Res Commun 306: 16-25, 2003.
14. Sung YK, Hwang SY, Park MK, *et al*: Glypican-3 is overexpressed in human hepatocellular carcinoma. Cancer Sci 94: 259-262, 2003.
15. Hippo Y, Watanabe K, Watanabe A, *et al*: Identification of soluble NH2-terminal fragment of glypican-3 as a serological marker for early-stage hepatocellular carcinoma. Cancer Res 64: 2418-2423, 2004.
16. Yamauchi N, Watanabe A, Hishinuma M, *et al*: The glypican 3 oncofetal protein is a promising diagnostic marker for hepatocellular carcinoma. Mod Pathol 18: 1591-1598, 2005.
17. Filmus J: The contribution of *in vivo* manipulation of gene expression to the understanding of the function of glypicans. Glycoconj J 19: 319-323, 2002.
18. De Cat B, Muyldermans SY, Coomans C, *et al*: Processing by proprotein convertases is required for glypican-3 modulation of cell survival, Wnt signaling and gastrulation movements. J Cell Biol 163: 625-635, 2003.
19. Capurro MI, Shi W, Sandal S and Filmus J: Processing by convertases is not required for glypican-3-induced stimulation of hepatocellular carcinoma growth. J Biol Chem 280: 41201-41206, 2005.
20. Capurro MI, Xiang YY, Lobe C and Filmus J: Glypican-3 promotes the growth of hepatocellular carcinoma by stimulating canonical Wnt signaling. Cancer Res 65: 6245-6254, 2005.
21. Song HH, Shi W, Xiang YY and Filmus J: The loss of glypican-3 induces alterations in Wnt signaling. J Biol Chem 280: 2116-2125, 2005.
22. Varma RR, Hector SM, Clark K, Greco WR, Hawthorn L and Pendyala L: Gene expression profiling of a clonal isolate of oxaliplatin-resistant ovarian carcinoma cell line A2780/C10. Oncol Rep 14: 925-932, 2005.
23. Filmus J, Capurro M and Rast J: Glypicans. Genome Biol 9: 224, 2008.
24. Stigliano I, Puricelli L, Filmus J, Sogayar MC, Bal de Kier Joffe E and Peters MG: Glypican-3 regulates migration, adhesion and actin cytoskeleton organization in mammary tumor cells through Wnt signaling modulation. Breast Cancer Res Treat (In press).
25. Torisu Y, Watanabe A, Nonaka A, *et al*: Human homolog of NOTUM, overexpressed in hepatocellular carcinoma, is regulated transcriptionally by beta-catenin/TCF. Cancer Sci 99: 1139-1146, 2008.
26. Jia HL, Ye QH, Qin LX, *et al*: Gene expression profiling reveals potential biomarkers of human hepatocellular carcinoma. Clin Cancer Res 13: 1133-1139, 2007.
27. Nakatsura T, Kageshita T, Ito S, *et al*: Identification of glypican-3 as a novel tumor marker for melanoma. Clin Cancer Res 10: 6612-6621, 2004.
28. Ikuta Y, Nakatsura T, Kageshita T, *et al*: Highly sensitive detection of melanoma at an early stage based on the increased serum secreted protein acidic and rich in cysteine and glypican-3 levels. Clin Cancer Res 11: 8079-8088, 2005.
29. Nakatsura T and Nishimura Y: Usefulness of the novel oncofetal antigen glypican-3 for diagnosis of hepatocellular carcinoma and melanoma. BioDrugs 19: 71-77, 2005.
30. Goodman ZD, Ishak KG, Langloss JM, Sesterhenn IA and Rabin L: Combined hepatocellular-cholangiocarcinoma: a histologic and immunohistochemical study. Cancer 55: 124-135, 1985.
31. Kassahun WT and Hauss J: Management of combined hepatocellular and cholangiocarcinoma. Int J Clin Pract (In press).
32. Taketa K: Alpha-fetoprotein: reevaluation in hepatology. Hepatology 12: 1420-1432, 1990.
33. Tangkijvanich P, Tosukhowong P, Bunyongyod P, *et al*: Alpha-L-fucosidase as a serum marker of hepatocellular carcinoma in Thailand. Southeast Asian J Trop Med Public Health 30: 110-114, 1999.
34. Filmus J and Capurro M: Glypican-3 and alphafetoprotein as diagnostic tests for hepatocellular carcinoma. Mol Diagn 8: 207-212, 2004.
35. Wee A: Fine needle aspiration biopsy of the liver: algorithmic approach and current issues in the diagnosis of hepatocellular carcinoma. Cytojournal 2: 7, 2005.
36. Man XB, Tang L, Zhang BH, *et al*: Upregulation of Glypican-3 expression in hepatocellular carcinoma but downregulation in cholangiocarcinoma indicates its differential diagnosis value in primary liver cancers. Liver Int 25: 962-966, 2005.
37. Tickoo SK, Zee SY, Obiekwe S, *et al*: Combined hepatocellular-cholangiocarcinoma: a histopathologic, immunohistochemical, and *in situ* hybridization study. Am J Surg Pathol 26: 989-997, 2002.
38. Yano Y, Yamamoto J, Kosuge T, *et al*: Combined hepatocellular and cholangiocarcinoma: a clinicopathologic study of 26 resected cases. Jpn J Clin Oncol 33: 283-287, 2003.
39. Nishie A, Yoshimitsu K, Asayama Y, *et al*: Detection of combined hepatocellular and cholangiocarcinomas on enhanced CT: comparison with histologic findings. AJR 184: 1157-1162, 2005.
40. Chu PG, Ishizawa S, Wu E and Weiss LM: Hepatocyte antigen as a marker of hepatocellular carcinoma: an immunohistochemical comparison to carcinoembryonic antigen, CD10, and alpha-fetoprotein. Am J Surg Pathol 26: 978-988, 2002.
41. Zhang F, Chen XP, Zhang W, *et al*: Combined hepatocellular cholangiocarcinoma originating from hepatic progenitor cells: immunohistochemical and double-fluorescence immunostaining evidence. Histopathology 52: 224-232, 2008.
42. Taguchi J, Nakashima O, Tanaka M, Hisaka T, Takazawa T and Kojiro M: A clinicopathological study on combined hepatocellular and cholangiocarcinoma. J Gastroenterol Hepatol 11: 758-764, 1996.
43. Wu PC, Fang JW, Lau VK, Lai CL, Lo CK and Lau JY: Classification of hepatocellular carcinoma according to hepatocellular and biliary differentiation markers. Clinical and biological implications. Am J Pathol 149: 1167-1175, 1996.

44. Nakatsura T, Komori H, Kubo T, *et al*: Mouse homologue of a novel human oncofetal antigen, glypican-3, evokes T-cell-mediated tumor rejection without autoimmune reactions in mice. Clin Cancer Res 10: 8630-8640, 2004.
45. Komori H, Nakatsura T, Senju S, *et al*: Identification of HLA-A2- or HLA-A24-restricted CTL epitopes possibly useful for glypican-3-specific immunotherapy of hepatocellular carcinoma. Clin Cancer Res 12: 2689-2697, 2006.
46. Motomura Y, Senju S, Nakatsura T, *et al*: Embryonic stem cell-derived dendritic cells expressing glypican-3, a recently identified oncofetal antigen, induce protective immunity against highly metastatic mouse melanoma, B16-F10. Cancer Res 66: 2414-2422, 2006.
47. Motomura Y, Ikuta Y, Kuronuma T, *et al*: HLA-A2 and -A24-restricted glypican-3-derived peptide vaccine induces specific CTLs: preclinical study using mice. Int J Oncol 32: 985-990, 2008.
48. Grozdanov PN, Yovchev MI and Dabeva MD: The oncofetal protein glypican-3 is a novel marker of hepatic progenitor/oval cells. Lab Invest 86: 1272-1284, 2006.
49. Durnez A, Verslype C, Nevens F, *et al*: The clinicopathological and prognostic relevance of cytokeratin 7 and 19 expression in hepatocellular carcinoma: a possible progenitor cell origin. Histopathology 49: 138-151, 2006.
50. Komuta M, Spee B, Vander Borght S, *et al*: Clinicopathological study on cholangiolocellular carcinoma suggesting hepatic progenitor cell origin. Hepatology 47: 1544-1556, 2008.
51. Fausto N and Campbell JS: The role of hepatocytes and oval cells in liver regeneration and repopulation. Mech Dev 120: 117-130, 2003.
52. Libbrecht L: Hepatic progenitor cells in human liver tumor development. World J Gastroenterol 12: 6261-6265, 2006.
53. Alison MR, Vig P, Russo F, *et al*: Hepatic stem cells: from inside and outside the liver? Cell Prolif 37: 1-21, 2004.

Gastric Cancer (2009) 12: 37–42
DOI 10.1007/s10120-008-0496-1

Original article

Phase II trial of S-1 for neoadjuvant chemotherapy against scirrhous gastric cancer (JCOG 0002)

TAIRA KINOSHITA[1], MITSURU SASAKO[2], TAKESHI SANO[3], HITOSHI KATAI[4], HIROSHI FURUKAWA[5], AKIRA TSUBURAYA[6], ISAO MIYASHIRO[7], MASAHIDE KAJI[8], and MOTOKI NINOMIYA[9] (on behalf of the Gastric Cancer Surgery Study Group of the Japan Clinical Oncology Group)

[1]Department of Surgical Oncology, National Cancer Center Hospital East, 6-5-1 Kashiwanoha, Kashiwa, Chiba 277-8577, Japan
[2]Department of Surgery, Hyogo College of Medicine, Kobe, Japan
[3]Department of Surgery, Cancer Institute Hospital, Tokyo, Japan
[4]Department of Surgical Oncology, National Cancer Center Hospital, Tokyo, Japan
[5]Department of Surgery, Sakai Municipal Hospital, Osaka, Japan
[6]Department of Surgical Oncology, Kanagawa Prefectural Cancer Center Hospital, Yokohama, Japan
[7]Department of Surgery, Osaka Medical Centre for Cancer and Cardiovascular Diseases, Osaka, Japan
[8]Department of Surgery, Toyama Prefectural Central Hospital, Toyama, Japan
[9]Department of Surgery, Hiroshima City Hospital, Hiroshima, Japan

Abstract

Background. **The prognosis of scirrhous gastric cancer remains poor despite extended surgery or adjuvant or neoadjuvant chemotherapy. A pilot study of S-1 (TS-1; Taiho Pharmaceutical, Tokyo, Japan), an oral 5-fluorouracil derivative, for neoadjuvant chemotherapy unexpectedly showed good response and a promising effect on survival. Therefore, the Japan Clinical Oncology Group conducted a phase II trial to confirm the efficacy of S-1 for neoadjuvant chemotherapy against resectable scirrhous gastric cancer.**

Methods. **Patients were eligible if they had typical scirrhous gastric cancer invading more than half of the stomach, and resectable disease confirmed by laparoscopic staging. The treatment schedule consisted of two courses (each, 4-week administration and 2-week withdrawal) of S-1 (100–120 mg/body per day), followed by radical surgery.**

Results. **Fifty-five eligible patients were registered. Three completed only one course of the neoadjuvant chemotherapy, whereas 52 completed two courses. Toxicity was acceptable, with a few grade 3 (5.5%) events, but no grade 4 adverse events. The response rate was 32.6% in 43 evaluable patients. Of the 55 patients, 2 refused operation, 1 developed lung metastasis, and 52 underwent laparotomy. The curative resection rate was 80.8%, with acceptable morbidity and no mortality. The survival curve at 2 years' follow up showed a better survival rate than that of the historical controls, but did not reach the expected survival rate.**

Conclusion. **S-1 neoadjuvant chemotherapy appeared feasible and showed positive effects against scirrhous gastric cancer; however, the survival rate with S-1 did not reach the expected rate required when selecting an agent for a phase III trial to confirm the effectiveness of neoadjuvant chemotherapy against scirrhous gastric cancer.**

Offprint requests to: T. Kinoshita

Received: September 16, 2008 / Accepted: November 27, 2008

Key words Scirrhous gastric cancer · Neoadjuvant chemotherapy · S-1

Introduction

Scirrhous gastric cancer, also known as linitis plastica or Borrmann type 4, is a special type of stomach cancer known for its very poor prognosis. It is very difficult to identify this cancer in its early stage, and even aggressive surgical procedures and adjuvant chemotherapies have not considerably improved the survival rate in patients with this neoplasia. Owing to its low incidence, only a few drug trials against this neoplasia have been conducted thus far. On the other hand, several studies of neoadjuvant chemotherapy against scirrhous gastric cancer have suggested the efficacy of such treatment [1–4]. However, all these studies involved a small sample size and they usually did not determine the survival benefits of such treatment. Furthermore, a phase II trial of sequential high-dose methotrexate and fluorouracil combined with doxorubicin (FAMTX) for neoadjuvant chemotherapy has shown moderate toxicity and no survival benefits [5]. Interestingly, S-1, which is a dihydropyrimidine dehydrogenase (DPD)-inhibitory fluoropyrimidine, has shown the highest response rate among many oral anticancer agents against unresectable advanced gastric cancer in early and late phase II trials [6–8]. In these late phase II trials, S-1 showed a 33% response rate against scirrhous gastric cancer. Because of the reported promising effects of S-1 for neoadjuvant chemotherapy against scirrhous gastric cancer in a previous pilot study [9], the Japan Clinical Oncology Group

(JCOG) decided to conduct a phase II trial to determine survival benefits of S-1 treatment.

Patients, materials and methods

Patient eligibility

Patient eligibility required the fulfillment of the following criteria: histologically confirmed gastric adenocarcinoma; potentially resectable laparoscopy-confirmed typical scirrhous gastric cancer (without definitive ulceration) that invaded more than half of the stomach; received no prior treatment; 70 years or younger; Eastern Cooperative Oncology Group performance status of 0 or 1; and oral intake possible. Patients also had to have adequate organ functions (creatinine clearance, ≥50 ml/min; blood urea creatinine, within the institutional limit; GOT and GPT, within twice the institutional limit; leukocytes, 3500/mm^3≤ leukocyte <12000/mm^3; hemoglobin, ≥9.0 g/dl; thrombocytes, ≥1000000/mm^3; total bilirubin, within twice the institutional limit; and normal electrocardiogram).

Diagnostic and staging procedures included physical examination, barium gastrography, endoscopy, chest X-ray, abdominal computed tomography (CT) scan, and laparoscopy with cytological examination of peritoneal washing of the Douglas pouch. Patients with positive cytology on peritoneal washing and potentially resectable disease without visible peritoneal dissemination were also included in the study.

This study was approved by the Institutional Review Board, and written informed consent was obtained from all patients.

Treatment schedule

Chemotherapy consisted of two courses (4-week administration and 2-week withdrawal) of S-1 at 100–120 mg/body per day. After two courses of neoadjuvant chemotherapy, patients were reevaluated for the presence of potentially resectable disease and those who were positive underwent laparotomy. Because two patients underwent endoscopic examination after one course of chemotherapy and stopped chemotherapy due to progressive disease, the treatment protocol was revised such that the evaluation of the effect of neoadjuvant chemotherapy should be carried out only after two courses and only by fluoroscopic examination. If indicated, patients received curative or palliative resection or exploratory laparotomy within 14 days after completing the second course of adjuvant chemotherapy. Patients with curative resection were followed up without any adjuvant chemotherapy every 3 months until cancer relapse.

Evaluation of response and toxicity

Potentially resectable scirrhous gastric cancer usually shows no measurable lesions, except for primary foci. We decided to evaluate the response of only primary foci following chemotherapy. Because it is very difficult to evaluate the response of the primary foci using the Response Evaluation Criteria in Solid Tumors criteria, we used a National Institutes of Health (NIH) image to calculate the barium-filling area or whole stomach on a double-contrast fluoroscopic examination study, as well as to compare the area before and after chemotherapy. Responses were classified as partial response (PR), more than 50% increase in the area after chemotherapy; stable disease (SD), 0 to less than 50% increase in the area; and progressive disease (PD), any decrease in the area and the appearance of new lesions. National Cancer Institute Common Toxicity Criteria ver2.0 were employed for determining chemotherapy toxicity.

Pathological assessment was performed to evaluate disease extent, resection margins, and response to chemotherapy as evidenced by the presence of necrotic and cancer cells. The pathological response to chemotherapy was classified according to the following criteria provided by the Japanese Gastric Cancer Association [10]: grade 0, absence of necrosis or degeneration; grade 1a, necrosis or degeneration is observed in less than one-third of the tumor; grade 1b, less than two-thirds and more than one-third of the tumor show necrosis or degeneration; grade 2, more than two-thirds of the tumor shows necrosis or degeneration; grade 3, all tumors show necrosis or degeneration.

Historical controls

Because we applied laparoscopic staging to exclude patients with visible peritoneal dissemination, it was very difficult to find good historical controls. Laparoscopic staging had gained popularity at the commencement of this trial; however, we had no identical historical controls. The historical controls consisted of 241 patients who had the same lesions as those described in the eligibility criteria for this study, and who had no visible peritoneal dissemination at laparotomy without laparoscopic staging, and had been treated at the participating institution during 1991–1993. Data for the historical controls were as follows: 2-year survival rate, 45%; curative resection rate, 90.3%; 30-day operative mortality rate, 1.2%; and in-hospital mortality rate, 3.5%.

Statistical considerations

The primary endpoint of this study was the 2-year survival rate. Fifty-five patients were required to be registered on the basis of the expectation that the 2-year survival rate of those receiving this neoadjuvant chemo-

therapy would be 60% (15% higher than that of the historical controls), allowing 10% of ineligible patients. Survival time was calculated from the initial date of the initiation of neoadjuvant chemotherapy to the date of death or the last follow-up date. Survival data were analyzed according to the method of Kaplan and Meier and then compared with the data of the historical controls.

Results

Patient accrual

From March 14, 2001, to February 4, 2003, 55 patients were enrolled in the study from 15 institutions. The mean age was 56 years (range, 31–70 years).

Neoadjuvant chemotherapy

The patients were composed of 26 male and 29 female patients. The scheduled two courses of neoadjuvant chemotherapy were performed in 52 patients. The remaining 3 patients received one course, because 2 of the 3 patients were judged to have PD by endoscopic evaluation after one course before the revision of the protocol, and 1 patient was found to have advanced bile duct carcinoma after one course of chemotherapy. These 3 patients received curative resection after one course of neoadjuvant chemotherapy. There was no chemotherapy-induced grade 4 adverse reaction in the cohort. Only 3 patients developed grade 3 adverse reactions (Table 1).

As mentioned earlier, the effect of adjuvant chemotherapy was evaluated from the change in the barium-filling area before and after the chemotherapy, as calculated from the NIH images. Among the 43 patients whose fluoroscopic films could be evaluated, 14 patients (32.6%) showed more than 1.5 times enlargement of the stomach (PR); 13 patients showed SD (30.2%), and 16 patients showed PD (37.2%).

Table 1. Adverse reactions

	Grade				%	
	0	1–2	3	4	Grade 4	Total
T. Bil	32	23	0	0	0	55
WBC	42	13	0	0	0	55
Neutrophils	42	12	1	0	0	55
ALT	43	11	2	0	0	55
AST	45	9	0	0	0	55
Hb	48	7	0	0	0	55
Nausea/vomiting	36	19	0	0	0	55
Pigmentation	44	11	0	0	0	55
Anorexia	45	10	0	0	0	55
Diarrhea	45	10	0	0	0	55
Stomatitis	45	10	0	0	0	55
General fatigue	46	9	0	0	0	55

Only three patients developed grade 3 adverse reactions, and they recovered by withdrawal of S-1

T. Bil, serum total bilirubin; WBC, white blood cell count; ALT, alanine aminotransferase; AST, aspartate aminotransferase; Hb, hemoglobin

Operation

Among the 55 patients, 3 did not undergo operation, because of the refusal of 2 and because the other patient was found to have pulmonary metastases. Fifty-two patients underwent laparotomy, including the 3 patients who received one course of the neoadjuvant chemotherapy. Among the 52 patients, 6 patients did not undergo resection (5, peritoneal dissemination; 1, unresectable invasion of the duodenum and pancreatic head). Ten patients underwent palliative resection of the main tumor (2, peritoneal dissemination; 6, positive cytological examination of abdominal washing; 1, unresectable tumor with severe invasion to the retroperitoneum; 1, widespread lymph node metastases). The other 36 patients underwent curative total gastrectomy with various combined organ resections (25, spleen; 1, distal pancreas + spleen; 5, gallbladder; 2, left adrenal gland; 2, transverse colon; 1, pancreatic head and duodenum). Among the 36 patients, only 1 had D1 lymph node dissection and the remaining 35 had D2 or more lymph node dissection.

The mean operation time for curative resection was 214 min (range, 130–460 min) and that for noncurative resection was 295 min (range, 150–401 min). The mean blood loss for curative resection was 586 ml (range, 30–1815 ml) and that for noncurative resection was 872 ml (range, 230–2100 ml).

Among the 46 patients who underwent resection, postoperative complications were observed in 11 patients (23.9%). Overall, there was no mortality and there were no serious complications. The actual complications were as follows: wound infection, deep vein thrombosis, pancreatic fistula, anastomotic ulcer, pneumonia, pulmonary embolism, sepsis, abdominal abscess, liver function disorder, and mycotic uveitis.

Changes in the T, P, and CY (cytological examination of the abdominal washing) factors before and after neoadjuvant chemotherapy are shown in Tables 2 and 3. With regard to the T factor, a response was observed in 14 patients; however, cancer progression was observed in 8 patients. In regard to the P and CY factors, a response (PR) was observed in only 2 patients; however, 10 showed progressive disease (PD). The other 40 patients showed stable disease (SD).

The pathological therapeutic effects of neoadjuvant chemotherapy were evaluated according the grading described by the Japanese classification of gastric carci-

noma [10] general rules for gastric cancer study: grade 0, 12 patients (26.1%); grade 1a, 19 patients (41.3%); grade 1b, 4 patients (8.7%), and grade 2, 11 patients (23.9%).

At the time of the scheduled analyses (March 2005), 10 patients were still alive without recurrence, 13 were alive with recurrence, and 32 had already passed away. The modes of recurrence were as follows: peritoneal, 17 patients; retroperitoneal, 2 patients; local, 1 patient; lymph node, 1 patient.

Table 2. Changes in T factors before and after chemotherapy

Laparoscopic T		Pathological T
T2:7		T2:11
T3:39	Chemotherapy	T3:37
T4:5		T4:4
Tx:1		

Progression, 8 patients; downstage, 14 patients
Tx, T unknown

Table 3. Changes in P and CY factors before and after chemotherapy

No change or progression (SD and PD)	
P0, CY0→P0,CY0	37 (SD)
P0, CY0→P0, CY1	2 (PD)
P0, CY1→P0, CY1	3 (SD)
P0, CY0→P1	4 (PD)
P0, CY1→P1	4 (PD)
Downstage (PR)	
P0, CY1→P0, CY0	2 (PR)

The survival curves of all patients (n = 55) and the historical controls are shown in Fig. 1. The survival curve of the study arm was better than that of the historical controls; however, the survival rate did not reach the expected rate (2-year survival rate: 59% vs 60%).

With regard to the secondary endpoints, the response rate to the neoadjuvant chemotherapy was 32.6%. The rate of postoperative complications was 23.9%, as against 25.7% in the historical controls. The in-hospital mortality rate was 0% as against 3.5% in the historical controls. The curative resection rate was 80.8%, as against 90.3% in the historical controls.

Discussion

Despite recent advances in chemotherapy and extended surgery, the treatment outcomes of scirrhous gastric cancer, also known as diffuse gastric cancer, linitis plastica, or Borrmann type 4 in the West, have remained very poor because of the aggressive biological behavior of this tumor. Because of failure to improve survival even with aggressive postoperative chemotherapy, neoadjuvant chemotherapy has been applied to patients with resectable or unresectable scirrhous gastric cancer.

To date, the efficacy of neoadjuvant chemotherapy against scirrhous gastric cancer remains to be established because of the lack of well-validated phase II and phase III studies. The first phase II neoadjuvant chemotherapy trial was reported by Takahashi et al., using FAMTX [5]. In their trial, neoadjuvant chemotherapy was shown to be seemingly feasible against scirrhous

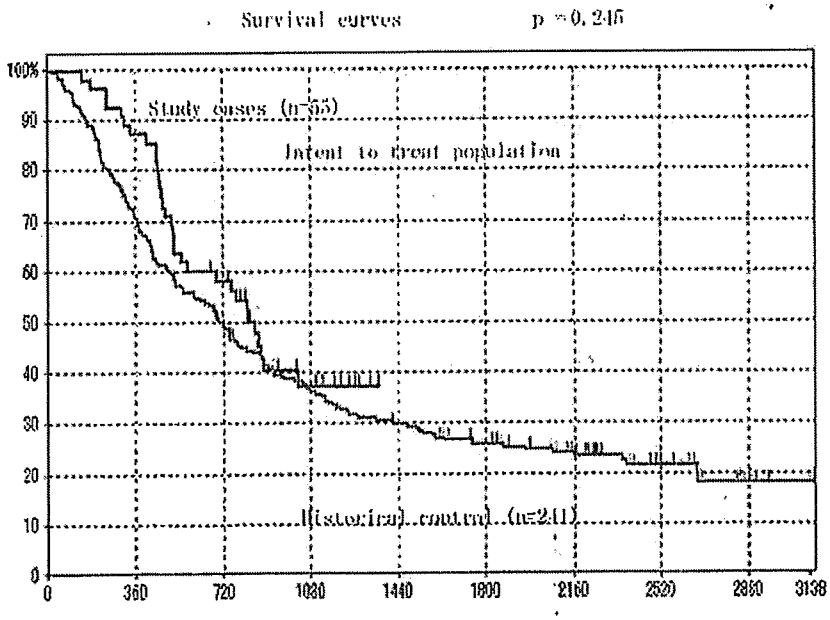

Fig. 1. Survival curves of all patients (n = 55) and the historical controls (n = 241)

gastric cancer, producing a higher resectability rate without any increase in morbidity rate. However, an interim analysis of the 2-year survival rate in 20 patients enrolled in the trial showed no improvement over the survival rate of the historical controls. Myelosuppression was the major cytotoxic effect of the FAMTX regimen, and grade 3 or 4 neutropenia was observed in 14 out of the 20 patients (70%). Eleven of these 14 patients required granulocyte colony-stimulating factor support. The overall response rate was 15% (3 PRs in 20 patients). Eighteen resected specimens showed only marginal histological effects (grades 0-Ib). For these reasons, Takahashi and co-workers discontinued the trial.

Because S-1 showed promising effects when used for neoadjuvant chemotherapy against scirrhous gastric cancer in a pilot study [9], we decided to conduct a phase II trial of S-1 to determine its beneficial effects on survival. Because of the difficulty in excluding patients with peritoneal dissemination by conventional diagnostic imaging procedures such as CT scan and the use of barium enema, we performed laparoscopic examination to identify and exclude patients with peritoneal dissemination.

At the time of starting the phase II trial, laparoscopic examination for cancer staging was still not a common procedure. Thus, we need to standardize this technique using a video for the quality control of the procedure. Regarding the historical controls, it was not possible to submit patients without peritoneal dissemination to laparoscopic examination, for the same reason. Data for previous patients with the same eligibility criteria and without peritoneal dissemination, confirmed by laparotomy, were collected from the participating institutions. Thus, in the present study, the control group was not identical to the study group.

Neoadjuvant chemotherapy using S-1 was safe and feasible when compared with other toxic combination chemotherapies. Only a few grade 3 and no grade 4 adverse reactions resulting from cytotoxicity were observed, and no specific morbidity and no increases in morbidity and mortality rates were seen when compared with the data in the historical controls.

Patients with positive cytological examination results were included in this phase II trial. This is the reason why we expected the S-1 neoadjuvant chemotherapy to produce negative cytological examination results. However, the results of the trial, in terms of cytological findings, were not very promising. Without considering the cytological examination results, it can be observed that although there was no significant difference in the curative resection rate between the study group and the historical control group, the curative resection rate in the study group was lower than the expected rate.

From the viewpoint of the pathological therapeutic effects of chemotherapy, S-1 neoadjuvant chemotherapy showed a much better therapeutic effect than FAMTX.

The survival rate of our study group showed a better curve than that of the historical controls; however, it did not reach the expected rate ($P = 0.245$). On the other hand, combination chemotherapy using S-1 and cisplatin (CDDP) showed a markedly high response rate (76%) in a phase II trial. Therefore, this combination can be considered more promising than S-1 monotherapy for neoadjuvant chemotherapy against scirrhous gastric cancer. The JCOG has also completed the accrual of patients evaluated in the phase II trial of neoadjuvant chemotherapy using the above S-1 and CDDP regimen for resectable scirrhous and more-than-8-cm giant type 3 gastric cancer. Because of the superiority of this regimen over S-1 monotherapy in terms of the response rate and pathological therapeutic effects, the JCOG group has already started a phase III trial to confirm the effectiveness of neoadjuvant chemotherapy using S-1 + CDDP as against extended surgery in patients with scirrhous or large type 3 gastric cancer.

In summary, neoadjuvant chemotherapy using S-1 against potentially resectable scirrhous gastric cancer appears feasible and effective; however, in the present phase II trial, the survival rate of the patients did not reach the expected rate. On the other hand, an S-1 + CDDP regimen is now being tested in a phase III trial by the JCOG group as a more promising neoadjuvant regimen.

Acknowledgments This study was supported by a Grant-in-Aid for Cancer Research and the Second Term Comprehensive Strategy for Cancer, both by the Ministry of Health, Labour and Welfare, Japan.

References

1. Mai M, Ogino T, Ueda H, Ooi A, Takahashi Y, Sawaguchi K, et al. Study on neoadjuvant chemotherapy of Borrmann 4 type carcinoma of the stomach and its clinical significance. Nippon Gan Chiryo Gakkai Shi (J Jpn Soc Cancer Ther) 1990;25:586–97.
2. Maeda O, Iwase H, Mamiya N, Nakamura M, Mizuno T, Nishio Y, et al. A case of scirrhous cancer of the stomach which survived for more than 5 years after neoadjuvant chemotherapy with UFT (uracil and tegafur) and cisplatin. Intern Med 2000;9:239–44.
3. Eriguchi M, Osada I, Fujii Y, Takeda Y, Yoshizaki I, Akiyama N, et al. Pilot study for preoperative administration of 1-OHP to patients with advanced scirrhous type gastric cancer. Biomed Pharmacother 1997;51:217–22.
4. Suga S, Iwase H, Shimada M, Nishio Y, Ichihara T, Ichihara S, et al. Neoadjuvant chemotherapy in scirrhous cancer of the stomach using uracil, tegafur and cisplatin. Intern Med 1996;35:930–6.
5. Takahashi S, Kinoshita T, Konishi M, Nakagohri T, Inoue K, Ono M, et al. Phase II study of sequential high-dose methotrexate and fluorouracil combined with doxorubicin as a neoadjuvant chemo-

therapy for scirrhous gastric cancer. Gastric Cancer 2001;4; 192–7.
6. Sugimachi K, Maehara Y, Horikoshi N, Shimada Y, Sakata Y, Miyachi Y et al. An early phase II study of oral S-1, a newly developed 5-fluorouracil derivation for advanced and recurrent gastrointestinal cancers. Oncology 1999;57:202–10.
7. Sakata Y, Ohtsu A, Horikoshi N, Sugimachi K, Mitachi Y, Taguchi T. Late phase II study of novel oral fluoropyrimidine anticancer drug S-1 (1 M tegafur-04 M gimestat-1 M otastat potassium) in advanced gastric cancer patients. Eur J Cancer 1998; 34:1715–20.
8. Koizumi W, Kurihara M, Nakano S, Hasegawa K. Phase II study of S-1, a novel oral derivative of 5-fluorouracil, in advanced gastric cancer. Oncology 2000;58:191–7.
9. Kinoshita T, Konishi M, Nakagohri T, Inoue K, Oda T, Takahashi S, et al. Neoadjuvant chemotherapy with S-1 for scirrhous gastric cancer. A pilot study. Gastric Cancer 2003;6:40–4.
10. Japanese Gastric Cancer Association. Japanese classification of gastric carcinoma—second English edition—. Gastric Cancer 1998;1:10–24.

Research Article

Quantitative Metabolome Profiling of Colon and Stomach Cancer Microenvironment by Capillary Electrophoresis Time-of-Flight Mass Spectrometry

Akiyoshi Hirayama,[1] Kenjiro Kami,[1] Masahiro Sugimoto,[1] Maki Sugawara,[1] Naoko Toki,[1] Hiroko Onozuka,[2] Taira Kinoshita,[2] Norio Saito,[2] Atsushi Ochiai,[2] Masaru Tomita,[1] Hiroyasu Esumi,[2] and Tomoyoshi Soga[1]

[1]Institute for Advanced Biosciences, Keio University, Tsuruoka, Yamagata, Japan and [2]National Cancer Center Hospital East, Kashiwa, Chiba, Japan

Abstract

Most cancer cells predominantly produce energy by glycolysis rather than oxidative phosphorylation via the tricarboxylic acid (TCA) cycle, even in the presence of an adequate oxygen supply (Warburg effect). However, little has been reported regarding the direct measurements of global metabolites in clinical tumor tissues. Here, we applied capillary electrophoresis time-of-flight mass spectrometry, which enables comprehensive and quantitative analysis of charged metabolites, to simultaneously measure their levels in tumor and grossly normal tissues obtained from 16 colon and 12 stomach cancer patients. Quantification of 94 metabolites in colon and 95 metabolites in stomach involved in glycolysis, the pentose phosphate pathway, the TCA and urea cycles, and amino acid and nucleotide metabolisms resulted in the identification of several cancer-specific metabolic traits. Extremely low glucose and high lactate and glycolytic intermediate concentrations were found in both colon and stomach tumor tissues, which indicated enhanced glycolysis and thus confirmed the Warburg effect. Significant accumulation of all amino acids except glutamine in the tumors implied autophagic degradation of proteins and active glutamine breakdown for energy production, i.e., glutaminolysis. In addition, significant organ-specific differences were found in the levels of TCA cycle intermediates, which reflected the dependency of each tissue on aerobic respiration according to oxygen availability. The results uncovered unexpectedly poor nutritional conditions in the actual tumor microenvironment and showed that capillary electrophoresis coupled to mass spectrometry–based metabolomics, which is capable of quantifying the levels of energy metabolites in tissues, could be a powerful tool for the development of novel anticancer agents that target cancer-specific metabolism. [Cancer Res 2009;69(11):4918–25]

Introduction

Most cancer cells are exposed to chronic hypoxia from the early stage of carcinogenesis. Indeed, the measurement of oxygen tension in tumors confirms severe hypoxia in many types of cancer (1). However, cancer cells' predominant use of glycolysis rather than oxidative phosphorylation for energy production, irrespective of oxygen availability (Warburg effect; ref. 2), is widely acknowledged. This indicates that tumor hypoxia is caused not by the excessive oxygen consumption of cancer cells, but rather the inadequate blood supply that results from structurally and functionally defective angiogenesis. In addition, intrinsic characteristics of cancer cells and their constitutive expression of hypoxia-inducible transcription factors activate the genes that encode glycolytic enzymes and glucose transporters (3, 4) and, therefore, jointly hyperactivate glycolysis, to replenish ATP for their continuous growth and proliferation. Nevertheless, the cancer cells' intense use of energy-inefficient glycolysis in the hypovascular microenvironment may deplete glucose from the surrounding tissues. In this manner, the nutritional conditions of the tumor microenvironment may be extremely unfavorable from the perspective of energy metabolism, and significantly different from those that we generally expect from the observation of overgrowing cancer cells.

Although little is known concerning the actual concentrations of glucose and resultant metabolic intermediates in human cancer tissues, the recent development of metabolomics technologies, which are typically based on gas chromatography mass spectrometry (GC-MS; ref. 5), liquid chromatography mass spectrometry (LC-MS; ref. 6), and nuclear magnetic resonance (NMR; ref. 7) is suitable for the large-scale measurement of metabolite levels in tumor and normal tissues. This provides not only direct information on energy metabolism but also the potential reciprocal relationship between metabolic networks and the underlying mechanisms of carcinogenesis.

Recently, metabolome analysis has been applied to the characterization of cancer-cell–specific metabolism. Yang and colleagues (8) applied a computational flux analysis to compare breast cancer and normal human mammary epithelial cell lines by using two-dimensional NMR and GC-MS. Their finding of significant increases in the glycine and proline biosynthesis in cancer cells is interesting, yet may be limited for *in vitro* environment due to its high dependency on culture conditions. Chan and colleagues (9) compared the metabolic profile of biopsied colorectal tumors and their matched normal mucosae obtained from 31 colorectal cancer patients using high-resolution magic angle spinning–NMR and GC-MS and obtained 31 marker metabolites that distinguish normal from malignant samples and further colon from rectal cancers. Moreover, applying GC-MS–based metabolomics, Denkert and colleagues (10) compared the metabolic profiles between invasive ovarian carcinomas and the borderline tumors and between colorectal tumor and pairwise normal tissues (11) and showed that differentially expressed metabolic phenotypes could be exploited

Note: Supplementary data for this article are available at Cancer Research Online (http://cancerres.aacrjournals.org/).

Requests for reprints: Tomoyoshi Soga, Institute for Advanced Biosciences, Keio University, Tsuruoka, Yamagata 997-0052, Japan. Phone: 81-235-29-0528; Fax: 81-235-29-0574; E-mail: soga@sfc.keio.ac.jp.

doi:10.1158/0008-5472.CAN-08-4806

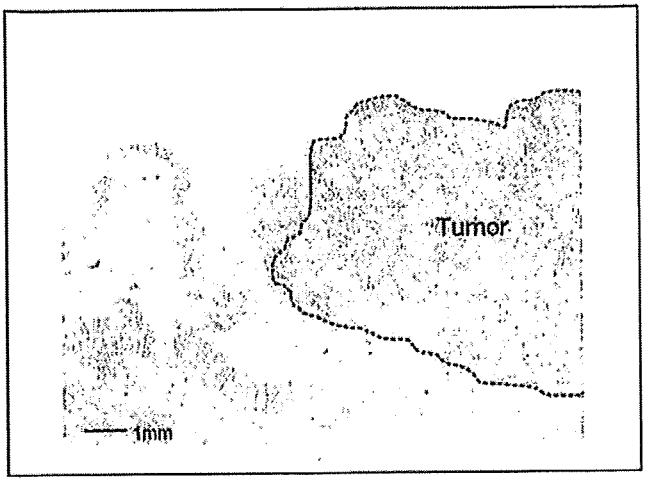

Figure 1. Representative microscopic image of an organ excised from a patient with well-differentiated colorectal adenocarcinoma. Samples were collected from the tumor region (*surrounded by a dotted line*) and nontumor region (considered normal).

to distinguish tumors from the others with high accuracies. However, little has been reported on the quantitation of metabolic intermediates involved in global-scale energy metabolism, including glycolysis, pentose phosphate pathway, and tricarboxylic acid (TCA) cycle, in human cancer and normal tissues. This is mainly due to the lack of effective methodology that allows comprehensive analysis of these metabolites. Most compounds involved in energy metabolism display common properties characterized by high polarity, nonvolatility, and poor detectability, which thus complicates the analysis. We recently developed a state-of-the-art metabolome analysis tool based on capillary electrophoresis coupled to mass spectrometry (CE-MS; refs. 12, 13). The major advantages of CE-MS analysis include its extremely high resolution, versatility to analyze metabolic profiles of various organisms, and ability to simultaneously quantify virtually all the charged low–molecular weight compounds in a sample (12, 14), which makes CE-MS best suited for the comprehensive analysis of energy metabolism in cells, tissues and biological fluids.

In the present study, we applied capillary electrophoresis time-of-flight mass spectrometry (CE-TOFMS; ref. 15) to the metabolome profiling of human colon and stomach cancers, and compared the metabolite levels in tumor and normal tissues obtained by surgery. The results clearly showed that the tumor microenvironment is far from ideal for cell growth from the viewpoint of energy metabolism, and showed the versatility of CE-MS–based metabolomics for global-scale analysis of energy metabolism in tissues.

Materials and Methods

Sample Collection and Metabolite Extraction

We conducted all the experiments according to the study protocol approved by the Institution Review Board of the National Cancer Center upon obtaining informed consent from all the subjects. Tumor and surrounding grossly normal-appearing tissues (Fig. 1) were obtained from 16 colon and 12 stomach cancer patients after surgical treatment. Patient and tumor stage information are listed in Table 1. The excised tissues were cut into <1-cm^3 pieces, immediately frozen in liquid nitrogen, and stored at −80°C until metabolite extraction.

To extract metabolites, preweighed deep-frozen samples (~50 mg each) were completely homogenized by a cell disrupter (MS-100R; TOMY) at 2°C, after adding 625 μL of methanol that contained internal standards [20 μmol/L each of methionine sulfone and 2-(N-morpholino)-ethanesulfonic acid]. The homogenate was then mixed with Milli-Q water and chloroform in a volume ratio of 5:2:5 and centrifuged at 9,000 *g* for 15 min at 4°C. Subsequently, the aqueous solution was centrifugally filtered through a 5-kDa cutoff filter (Millipore) to remove proteins. The filtrate was centrifugally concentrated and dissolved in 50 μL Milli-Q water that contained reference compounds (200 μmol/L each of 3-aminopyrrolidine and trimesate) immediately before CE-TOFMS analysis.

Reagents

Ophthalmate was purchased from BACHEM AG; glycerol-3-phosphate from Nakalai Tesque; sedoheptulose 7-phosphate from Glycoteam; tyramine, CoA, and NADH from MP Biomedicals; and fructose 1,6-bisphosphate, glucose 1-phosphate, ribose 5-phosphate, and ribulose 5-phosphate from Fluka. γ-Glu-Cys and γ-Glu-2-aminobutyrate were synthesized at the Toray Research Center. All other reagents were obtained from either Wako or Sigma-Aldrich. Stock solutions (1–100 mmol/L) were prepared in either Milli-Q water, 0.1 mol/L HCl, or 0.1 mol/L NaOH. All chemical standards were analytic or reagent grade. A mixed solution of the standards was prepared by diluting stock solutions with Milli-Q water immediately before CE-TOFMS analysis.

Analytic Condition for Metabolome Analysis

Instruments. All CE-TOFMS experiments were performed using an Agilent CE Capillary Electrophoresis System equipped with an Agilent TOFMS, an Agilent 1100 isocratic HPLC pump, an Agilent G1603A CE-MS adapter kit, and

Table 1. Patient information and tumor stages

Characteristic		Colon		Stomach	
		Number	%	Number	%
Position of colon tumor	Rectum	10	63		
	Ascending colon	3	19		
	Transverse colon	1	6		
	Sigmoid colon	2	13		
Stage	I	5	31	2	17
	II	4	25	3	25
	III	6	38	5	42
	IV	1	6	2	17
Sex	Male	11	69	7	58
	Female	5	31	5	42

an Agilent G1607A CE-electrospray ionization (ESI)-MS sprayer kit (Agilent Technologies). For system control and data acquisition, we used Agilent G2201AA ChemStation software for CE and Analyst QS for TOFMS.

For measuring nucleotide derivatives, we used a CE-ESI-quadrupole MS system composed of an Agilent 1100 series MSD mass spectrometer equipped with the aforementioned other instruments. For the control and data acquisition in this system, we used Agilent 3D CE-MSD ChemStation software.

CE-TOFMS Conditions for Cationic Metabolite Analysis

Cationic metabolites were separated in a fused-silica capillary (50 μm i.d. × 100 cm total length) filled with 1 mol/L formic acid as the reference electrolyte (16). Sample solution was injected at 50 mbar for 3 s (~3 nL), and positive voltage of 30 kV was applied. The capillary and sample trays were maintained at 20°C and below 5°C, respectively. Sheath liquid that comprised methanol/water (50% v/v) that contained 0.5 μmol/L reserpine was delivered at 10 μL/min. ESI-TOFMS was operated in the positive ion mode. The capillary voltage was set at 4 kV and a flow rate of nitrogen gas (heater temperature 300°C) was set at 10 psig. In TOFMS, the fragmenter voltage, skimmer voltage, and octapole radio frequency voltage (Oct RFV) were set at 75, 50, and 125 V, respectively. An automatic recalibration function was performed by using two reference masses of reference standards; protonated methanol dimer ($[2\ methanol+H]^+$, m/z 65.059706) and protonated reserpine ($[M+H]^+$, m/z 607.280659), which provided the lock mass for exact mass measurements. Exact mass data were acquired at the rate of 1.5 cycles/s over a 50 to 1,000 m/z range.

CE-TOFMS Conditions for Anionic Metabolite Analysis

Anionic metabolites were separated in a cationic-polymer-coated SMILE(+) capillary (Nacalai Tesque) filled with 50 mmol/L ammonium acetate solution (pH 8.5) as the reference electrolyte (13). Sample solution was injected at 50 mbar for 30 s (~30 nL) and a negative voltage of −30 kV was applied. Ammonium acetate (5 mmol/L) in 50% methanol/water (50% v/v) that contained 1 μmol/L reserpine was delivered as sheath liquid at 10 μL/min. ESI-TOFMS was operated in the negative ion mode. The capillary voltage was set at 3.5 kV. In TOFMS, the fragmenter voltage, skimmer voltage, and Oct RFV were set at 100, 50, and 200 V, respectively. An automatic recalibration function was performed by using two reference masses of reference standards: deprotonated acetate dimer ($[2M-H]^-$, m/z 119.034984) and deprotonated reserpine ($[M-H]^-$, m/z 607.266107). Other conditions were identical to those used in cationic metabolome analysis.

CE-MS Conditions for Nucleotide-Related Metabolite Analysis

Separations were carried out in a fused-silica capillary (50 μm i.d. × 100 cm total length) filled with 50 mmol/L ammonium acetate solution (pH 7.5) as electrolyte (17). Before the first use, a new capillary was pretreated with preconditioning buffer, 25 mmol/L ammonium acetate/75 mmol/L sodium phosphate solution (pH 7.5), for 20 min. Before each injection, the capillary was equilibrated by flushing with the preconditioning buffer for 10 min and subsequently with the running buffer for 6 min, which was replenished every run using a buffer replenishment system equipped with the Agilent CE. Sample solution was injected at 50 mbar for 30 s (~30 nL). A voltage of +30 kV was applied and a pressure of 50 mbar was applied to the inlet capillary during the run (17). The capillary temperature was maintained at 20°C, and the sample tray was cooled to below 5°C. Ammonium acetate (5 mmol/L) in 50% methanol/water (v/v) was delivered as the sheath liquid at 10 μL/min. ESI-quadrupole MS was operated in the negative ion mode, and the capillary voltage was set at 3.5 kV. A flow of heated dry nitrogen gas (heater temperature 300°C) was switched off during the preconditioning step, and a pressure of 10 psig was applied 0.1 min after sample injection. Compounds were monitored using selective ion monitoring mode.

Liquid Chromatography Tandem Mass Spectrometry Conditions for Glucose Quantification

Liquid chromatography tandem mass spectrometry experiments were performed using an Agilent 1100 series HPLC system and an API3000 triple-quadrupole tandem mass spectrometer (Applied Biosystems), with the Applied Biosystems Analyst software for data acquisition. The separation was carried out on a TSKgel Amide-80 column (2.1 mm i.d. × 25 cm; Tosoh) and the mobile phase consisted of 75% acetonitrile and 25% Milli-Q water at a flow-rate of 0.2 mL/min. The temperature of the column oven was set at 80°C and 1-μL aliquots of the sample solution were injected into the column. Turbo spray mode was selected in the negative ion mode. Nebulizer gas pressure, air curtain gas pressure, nitrogen turbo gas temperature, and ion spray voltage were set at 12 psig, 6 psig, 500°C, and −4.5 kV, respectively. Multiple reaction monitoring detection was performed in MS/MS analysis to obtain sufficient selectivity and sensitivity.

CE-TOFMS Data Processing

Raw data were processed using in house software for the quantitation of metabolites. The overall data processing flow consists of the following steps; noise-filtering, baseline-correction, migration time alignment, peak detection, and integration of peak area from a 0.02 m/z-wide slice of the electropherograms, which resemble the strategies used in widely used data processing software for LC-MS and GC-MS data analysis such as MassHunter (Agilent Technologies) and XCMS (18). Subsequently, the accurate m/z of each peak was calculated by Gaussian curve fitting in the m/z domain, and migration times were normalized using alignment algorithms based on dynamic programming (15, 19). All target metabolites were identified by matching their m/z values and migration times with those of the standard compounds. Processed peak lists were exported for further statistical analysis.

Statistical Analysis

For each sample, the measured metabolite concentrations were normalized using tissue weight to obtain the amount of metabolite contained per gram of each sample. The Wilcoxon matched pairs test was used to compare metabolite levels in tumor and nontumor groups, to determine statistical significance. Z-score normalization was performed and heat maps of metabolite levels were generated using hierarchical clustering based on Pearson correlation coefficients using the MultiExperiment Viewer (MeV) software (Institute for Genomic Research; ref. 20).

Results and Discussion

Metabolome analyses of colon and stomach cancer tissues. We obtained pairs of surgically resected tumor and surrounding normal tissue samples from 16 colon and 12 stomach cancer patients and extracted metabolites for metabolome analysis. Surgically excised tissue samples were immediately frozen in liquid nitrogen, quickly weighed and immersed in methanol with internal standards, and completely homogenized at 2°C, which thus minimized sample degradation and halted potential enzymatic reactions during metabolite extraction process.

The CE-TOFMS systems in three different modes for cation, anion, and nucleotide analyses detected 738 (normal) and 877 (tumor) peaks in colon and 1007 (normal) and 1142 (tumor) peaks in stomach tissues on average, after eliminating redundant peaks, such as spike noises, fragments, and adduct ions. Among these, 94 peaks in colon and 95 peaks in stomach were identified and quantified with metabolite standards by matching the closest m/z values and normalized migration times for further statistical comparisons and interpretations. The identified metabolites and their quantities are listed in Supplementary Table S1 and graphically represented on a large-scale metabolome map (Supplementary Fig. S1).

The relative levels of metabolites in normal and tumor tissues obtained from colon and stomach cancer patients were visualized by using a hierarchical clustering algorithm (Supplementary Fig. S2). The normalized metabolome data were clustered according to metabolites vertically and samples horizontally. Two distinct metabolite clusters were observed in colon tissues: Most

metabolite levels including glycolytic intermediates, amino acids, some TCA and urea cycle intermediates, and nucleosides were higher in tumor tissues compared with their normal counterparts; however, these clusters were less distinguishable in stomach tissues. This trend was also present in the sample clusters: Colon samples were clearly separated into tumor and normal groups except for one normal sample clustered within the tumor group, whereas stomach samples were not well-separated. This indicates that tumor and normal stomach tissues were less distinguishable compared with colon tissues, according to the metabolome data obtained in this study. However, several key metabolites in energy metabolism, such as glucose and nucleoside triphosphates, were lower in both colon and stomach tumor tissues. No significant correlation was found between metabolite levels and the cancer stages of patients in both tissue types (data not shown).

Glycolysis and TCA cycle. As expected from the notion that cancer cells can deplete glucose in the hypovascular microenvironment caused by the hyperactivity of glycolysis, glucose concentrations were much lower in tumor than normal tissues in both types of cancers (Fig. 2). Mean glucose concentration of normal and tumor tissues was 1,220 ± 150 (mean ± SE) and 123 ± 43 nmol/g, respectively, in colon (P = 0.0005) and 1,290 ± 168 and 424 ± 131 nmol/g, respectively, in stomach (P = 0.0068) tissues. Concentrations of metabolites that are involved in glycolysis, pentose phosphate pathway, and TCA cycle are illustrated on a metabolic pathway map in Fig. 3. In colon and stomach cancer, tumor tissues contained nearly equal or higher amounts of glycolytic intermediates than their corresponding normal counterparts, and this trend was clearer in colon tissues. Scarce glucose and modest glucose 6-phosphate concentrations might result from the overexpression of glucose transporters (21) and particularly type II hexokinase expression (22), which are frequently observed in colon and stomach cancer. The accumulation of glucose 1-phosphate in colon cancer is also intriguing in that glycogen synthase kinase 3β expression is reportedly higher in colon cancer cell lines and colorectal cancer patients compared with their respective normal counterparts (23), which may result in the enhancement of glycogenolysis and a continuous supply of glucose 6-phosphate.

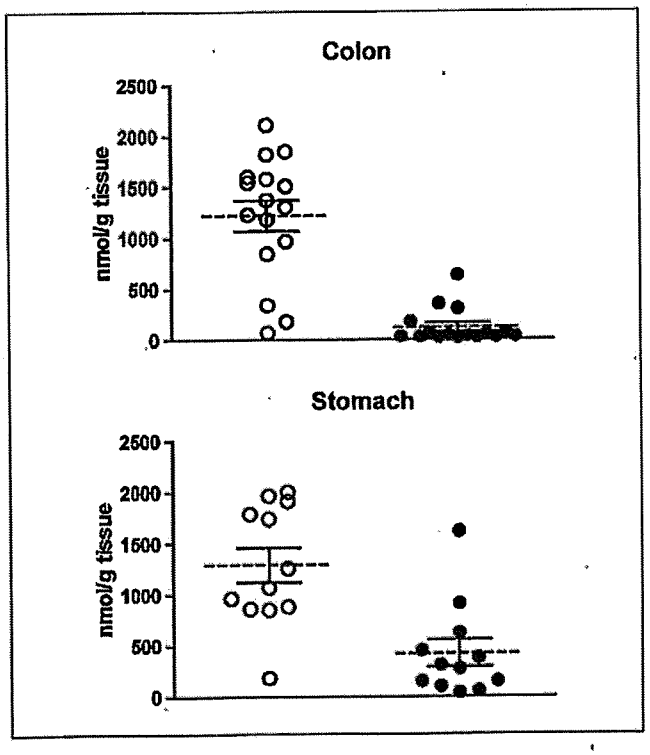

Figure 2. Quantified glucose concentrations of colon and stomach tissue samples. These data are individual glucose concentrations of normal and tumor samples each of colon and stomach subjects, with the mean concentrations (*dotted line*) ± SE.

In addition, pyruvate concentration is significantly lower in colon tumor and slightly lower in stomach tumor tissues, whereas lactate concentration in tumor tissues is higher in both tumor types than in their corresponding normal counterparts. This clearly indicates a high dependence of cancer cells on anaerobic breakdown of pyruvate. In particular, high lactate dehydrogenase 5 activity and resulting effective conversion of pyruvate to lactate have been identified in colon cancer (24, 25). Active glycolysis also increases the cytosolic NADH/NAD^+ ratio and thereby accelerates the activity of lactate dehydrogenase (26). Enhanced pyruvate-to-lactate conversion may also be due to the activation of pyruvate dehydrogenase kinase, isozyme 1 (PDK1) in cancer cells, which inactivates pyruvate dehydrogenase and leads to inactivation of the TCA cycle in cancer cells (27). Moreover, lactate accumulation creates a potentially favorable microenvironment for cancer cells to proliferate, as it causes local acidosis and potentially modulates the activity of proteases that decompose extracellular matrix, thereby liberating peptides and amino acids that are consumable for energy generation (28). Therefore, it is likely that cancer cells preferentially use glucose because of their intrinsic metabolic characteristics and microenvironmental aspects such as hypoxia. Moreover, extremely low glucose content in tumor tissues might result from poor blood supply and high glucose consumption by cancer cells.

If the density of soft tissues is assumed as 1 g/mL, our data indicate that the glucose concentration in tumor tissues is only ~1 of 45 (colon) or 1 of 13 (stomach) of the typical blood glucose concentration (1 mg/mL or 5.6 mmol/L). When cultured cancer cells are deprived of glucose, most conventional cytotoxic anticancer agents significantly lose their effectiveness (29). This is important when the pharmacologic effects of anticancer agents in the actual tumor microenvironment are considered since it was found to be significantly different from the typical glucose-rich medium that is commonly used for *in vitro* experiments. Accordingly, the present data imply that responses of most colon and stomach cancer cells against conventional anticancer drugs under the actual nutritionally poor *in vivo* environment could be considerably different from that which we expect from the data obtained under typical culture conditions.

Unexpectedly, significant organ-specific differences were also observed in the metabolite levels of the initial part of the TCA cycle, including acetyl CoA, citrate, *cis*-aconitate, iso-citrate, and 2-oxoglutarate, which were markedly lower in colon tissues. Interestingly, however, levels of the three TCA metabolites succinate, fumarate, and malate were comparable in colon and stomach tissues, whereas they were significantly higher in tumor samples in both cancers (Fig. 3). Wiesner and colleagues (30) have shown a decrease of citrate and 2-oxoglutarate and an increase of malate and succinate in anoxic rat heart myocytes. The trend of these TCA intermediate levels is consistent with our data obtained from colon tissues, presumably representing a typical metabolic fingerprint of hypoxic cells. In contrast, abundant TCA

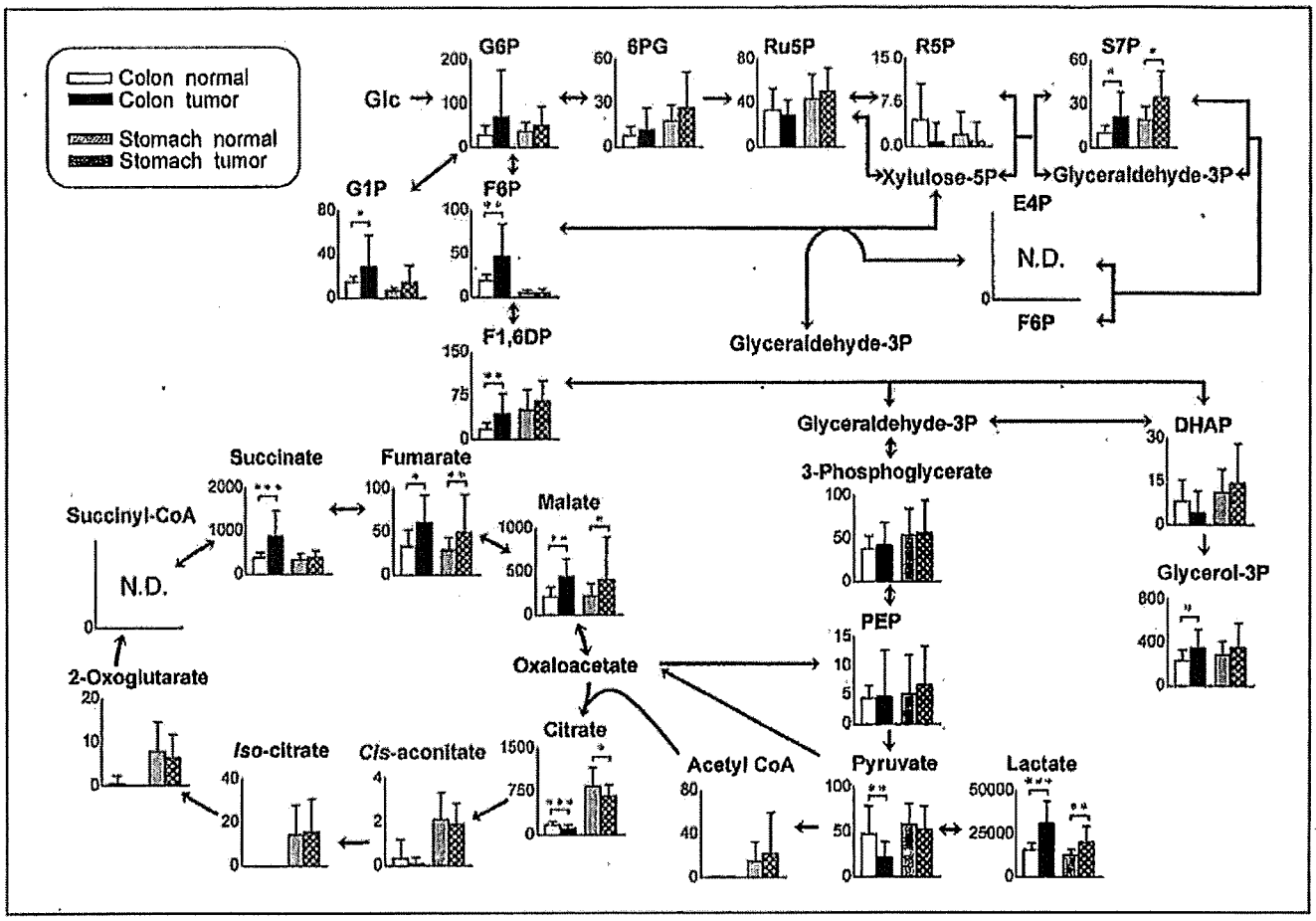

Figure 3. Quantified levels of metabolites involved in central carbon metabolism. Metabolite concentrations of colon and stomach tissues superimposed on a metabolic pathway map that included glycolysis, and the pentose phosphate and TCA pathways. *Columns*, average concentration (nmol/g tissue); *bars*, SD. *N.D.*, the metabolite concentration was below the detection limit of the analysis. All the *P* values were evaluated by the Wilcoxon matched pair test. *, $P < 0.05$; **, $P < 0.01$; ***, $P < 0.001$.

intermediates in stomach tissues, regardless of whether from tumor or normal tissues, imply active aerobic respiration via oxidative phosphorylation. It is uncertain, however, what causes the accumulation of fumarate and succinate in colon cancer tissues, despite extremely low concentrations of other TCA intermediates such as citrate and 2-oxoglutarate. In fact, it is known that some parasites and bacteria synthesize ATP without oxygen by using a reverse reaction of succinate dehydrogenase and produce succinate as a byproduct, which is so-called fumarate respiration, in which fumarate rather than molecular oxygen is used as electron acceptor (31, 32). Although the capability of mammalian cells to use fumarate respiration as an ATP generator has not been confirmed yet, we obtained strong evidence that the energy generation of cancer cells greatly depends on fumarate respiration under conditions of glucose deprivation and severe hypoxia.[3] Our data uncovered the metabolically unfavorable microenvironment of tumor tissues characterized by extremely low glucose availability under relatively hypoxic conditions in which the cells apparently rely on minimal aerobic respiration via the TCA cycle. Hence, the active use of fumarate respiration by cancer cells provides a likely and intriguing explanation for the accumulation of fumarate and succinate observed in colon tumor tissues.

Amino acids and nucleotides. Availability of amino acids is pivotal for cell proliferation because cancer cells are known to use some amino acids as energy sources (26). Free amino acids are mostly supplied to tissues via the bloodstream; thus, if blood supply to cancer tissues is considerably limited, amino acid content in tumor tissues may be lower compared with that in their normal counterparts. However, contrary to our expectations, levels of most amino acids and their primary derivatives were significantly higher in tumors than in normal colon and stomach tissues (Fig. 4). Among all the amino acids, however, an exception was glutamine; the colon and stomach tumor content of which was nearly equal to that in normal tissues. It has been pointed out that glutamine is a preferred amino acid for energy generation by cancer cells (33). High glutaminase activity and low glutamine synthase activity have been observed in several types of cancer cells (34). Because glutamate is the most abundant amino acid in tumor tissues, the conversion of glutamine to glutamate might be enhanced in tumor tissues.

One obvious question raised is the origin of these amino acids. Under limited blood supply, two main sources of amino acids can

[3] K. Kami et al. submitted for publication.

be conceived: one is the degradation of extracellular matrix particularly by matrix metalloproteinases and the other is the autophagic degradation of preexisting intracellular proteins. In this perspective, it is notable that hydroxyproline concentration was significantly higher in tumor tissues than in their normal counterparts (P = 0.0005 in colon and P = 0.0025 in stomach tissues). Hydroxyproline is abundant in collagen and is posttranslationally produced from proline, which suggests that the higher concentration of hydroxyproline in tumor tissues is indicative of excess degradation of collagen (35). Autophagy is another possible source of amino acids, as it is well-documented that autophagy liberates and thereby increases the free amino acid pools (36, 37). We also have found recently that autophagy seems essential for colon cancer cell survival (38) and is highly active in colon and pancreatic cancers (38, 39). Up-regulation of amino acid biosynthesis per se does not explain the accumulation of all the essential amino acids observed in tumor tissues. One might argue that all the amino acid levels seem to be higher in tumors because the number of cells contained in tumor tissues might have been greater than that in normal tissues, as cancer cells may have been highly aggregated. To rule out this possibility, we extracted DNA simultaneously with metabolites from each tissue and normalized our metabolome data with respect to the DNA content of each sample, and confirmed that the trend in amino acid levels did not change (data not shown).

The levels of most nucleotides such as ATP, ADP, GTP, and GDP in tumor and normal colon tissues were significantly lower than those in stomach tissues (Fig. 4). Nevertheless, no significant difference between colon and stomach tissues was observed with regard to the average adenylate energy charge (40), which is evaluated by the equation, [(ATP)+1/2(ADP)]/[(ATP)+(ADP)+(AMP)]. The low levels of most purine and pyrimidine compounds in colon tissues may indicate a relatively slower colon cell growth compared with stomach cells, as a recent study has shown that the nucleotide pools continuously decrease as the growth stage moves from the exponential to stationary phase in *Escherichia coli* (41). A challenging but intriguing alternative is that the levels of nucleotide pools may reflect the oxygen availability and its dependency in each tissue because hypoxic stress has been found to reduce purine and pyrimidine pools (42). The high-energy charge in colon tissues, despite the low total adenylate level, might be maintained by AMP deaminase reaction, which is known to stabilize the energy charge by decomposing adenylate (43). It is, however, remarkable that no significant difference between tumor and normal tissues was found for most nucleotide phosphates, total adenylate, and energy charge in either colon or stomach tissues. This implies that cancer cells have a growth advantage over their normal counterparts, not by securing more ATP and other building blocks for DNA synthesis, but rather by efficiently exploiting some strategic energy

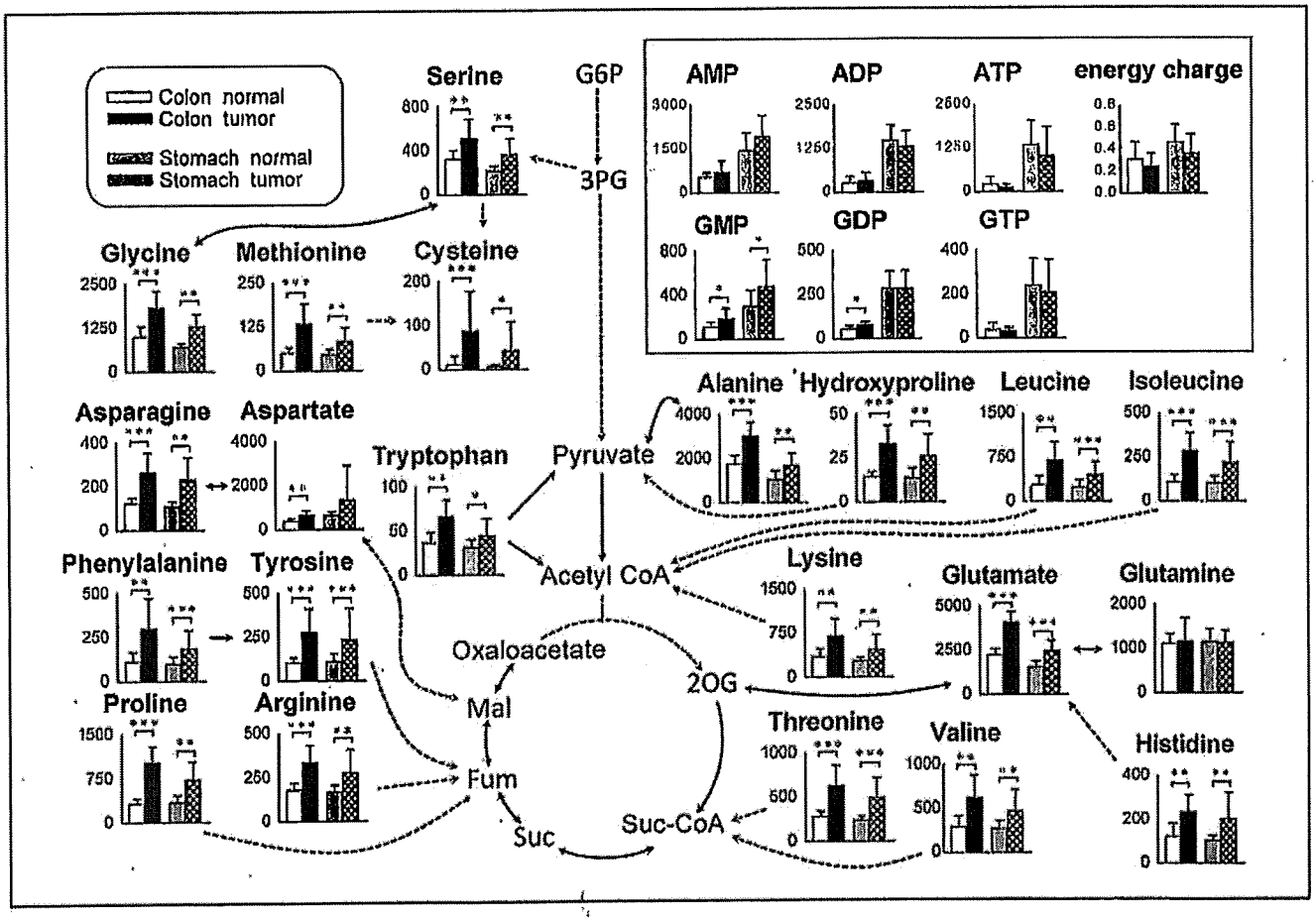

Figure 4. Metabolome data map of metabolites including amino acids, hydroxyproline, and nucleotides (shown in the box) in normal and tumor tissues obtained from colon and stomach cancer patients. *Columns*, average concentration (nmol/g tissue) of normal and tumor tissues; *bars*, SD. *N.D.*, the metabolite concentration was below the detection limit of the analysis. All the P values were evaluated by the Wilcoxon matched pair test. *, $P < 0.05$; **, $P < 0.01$; ***, $P < 0.001$.

metabolisms such as anaerobic glycolysis, glutaminolysis, autophagic production of amino acids, and possibly fumarate respiration, to maintain comparable levels of principal molecules in spite of limited resources and support continuous proliferation.

Intrasample variability and analytic limitations. Biochemical analysis of tissue samples is relatively difficult due to their high heterogeneity compared with cultured cells or body fluids. To examine the intrasample variability, we extracted metabolites from five different parts of a piece of colon or stomach tumor tissue and measured the metabolite levels by CE-TOFMS (Supplementary Table S2). The relative SDs of most metabolite levels were in the range of 6.7% to 40%. Given that the analytic variability of CE-MS is <5% (16), this relatively high intrasample variability may be attributed to a significantly high intratumor heterogeneity. Therefore, to minimize intrasample variability and thus maximize sensitivity for detecting tumor-specific or even tumor-stage specific metabolic differences, the use of laser capture microdissection for concentrating only the target cells before sample homogenization may be promising.

CE-MS is able to simultaneously quantify charged, low–molecular weight compounds and, thus, is suitable for the analysis of primary energy metabolism; however, it is not very effective for the separation of neutral compounds and macromolecules such as sugars, fats, cholesterols, steroid hormones, and long-chain peptides. Concomitant analysis of the same samples by LC-MS, GC-MS, and NMR approaches has the potential to greatly expand the coverage of target compounds and thereby increase the chance of finding molecular fingerprints of tumors and key markers of the tumorigenic process.

In the present study, we analyzed the metabolic state of tumor tissues in comparison with their normal counterparts and found that the nutritional conditions in the tumor microenvironment were far from ideal from the standpoint of energy metabolism. In particular, tumor glucose concentration was significantly lower than previously indicated (44). The results also indicate that tumors develop tumor-specific metabolism that endows them with more predominant proliferation, independent of tissue types, while retaining some metabolic traits of the tissues from which they originated. In other words, cancer cells are evolved through metabolic adaptation that involves primarily hyperactivation of glucose consumption and accumulation of amino acids, while retaining tissue-specific dependency of aerobic respiration represented by TCA intermediate and nucleotide levels. In conclusion, we analyzed the metabolome-wide tumor microenvironment and revealed cancer- and organ-specific characteristic energy metabolism by CE-TOFMS, which will be a vital technology for the future discovery of tissue-specific cancer biomarkers and for the awaited development of novel cancer therapeutic agents that target cancer-specific metabolic traits.

Disclosure of Potential Conflicts of Interest

No potential conflicts of interest were disclosed.

Acknowledgments

Received 12/17/08; revised 3/9/09; accepted 3/20/09; published OnlineFirst 5/19/09.

Grant support: Third Term Comprehensive 10-year Strategy for Cancer Control from the Ministry of Health, Labour and Welfare and a grant from the Global COE Program entitled, "Human Metabolomic Systems Biology." This work was also supported by KAKENHI (Grant-in-Aid for Scientific Research) on Priority Areas "Systems Genomes" and on "Lifesurveyor" from the Ministry of Education, Culture, Sports, Science and Technology of Japan as well as research funds from the Yamagata prefectural government and the City of Tsuruoka.

The costs of publication of this article were defrayed in part by the payment of page charges. This article must therefore be hereby marked *advertisement* in accordance with 18 U.S.C. Section 1734 solely to indicate this fact.

References

1. Vaupel P, Thews O, Kelleher DK, Konerding MA. O2 extraction is a key parameter determining the oxygenation status of malignant tumors and normal tissues. Int J Oncol 2003;22:795–8.
2. Warburg O. On the Origin of Cancer Cells. Science 1956;123:309–14.
3. Chen Z, Lu W, Garcia-Prieto C, Huang P. The Warburg effect and its cancer therapeutic implications. J Bioenerg Biomembr 2007;39:267–74.
4. Kondoh H. Cellular life span and the Warburg effect. Exp Cell Res 2008;314:1923–8.
5. Schauer N, Semel Y, Roessner U, et al. Comprehensive metabolic profiling and phenotyping of interspecific introgression lines for tomato improvement. Nat Biotechnol 2006;24:447–54.
6. Plumb R, Granger J, Stumpf C, Wilson ID, Evans JA, Lenz EM. Metabonomic analysis of mouse urine by liquid-chromatography-time of flight mass spectrometry (LC-TOFMS): detection of strain, diurnal and gender differences. Analyst 2003;128:819–23.
7. Opstad KS, Bell BA, Griffiths JR, Howe FA. An assessment of the effects of sample ischaemia and spinning time on the metabolic profile of brain tumour biopsy specimens as determined by high-resolution magic angle spinning 1H NMR. NMR Biomed 2008;21:1138–47.
8. Yang C, Richardson AD, Smith JW, Osterman A. Comparative metabolomics of breast cancer. Pac Symp Biocomput 2007:181–92.
9. Chan EC, Koh PK, Mal M, et al. Metabolic profiling of human colorectal cancer using high-resolution magic angle spinning nuclear magnetic resonance (HR-MAS NMR) spectroscopy and gas chromatography mass spectrometry (GC/MS). J Proteome Res 2009;8:352–61.
10. Denkert C, Budczies J, Kind T, et al. Mass spectrometry-based metabolic profiling reveals different metabolite patterns in invasive ovarian carcinomas and ovarian borderline tumors. Cancer Res 2006;66:10795–804.
11. Denkert C, Budczies J, Weichert W, et al. Metabolite profiling of human colon carcinoma-deregulation of TCA cycle and amino acid turnover. Mol Cancer 2008;7:72.
12. Soga T, Ohashi Y, Ueno Y, Naraoka H, Tomita M, Nishioka T. Quantitative metabolome analysis using capillary electrophoresis mass spectrometry. J Proteome Res 2003;2:488–94.
13. Soga T, Ueno Y, Naraoka H, Ohashi Y, Tomita M, Nishioka T. Simultaneous determination of anionic intermediates for Bacillus subtilis metabolic pathways by capillary electrophoresis electrospray ionization mass spectrometry. Anal Chem 2002;74:2233–9.
14. Sato S, Soga T, Nishioka T, Tomita M. Simultaneous determination of the main metabolites in rice leaves using capillary electrophoresis mass spectrometry and capillary electrophoresis diode array detection. Plant J 2004;40:151–63.
15. Soga T, Baran R, Suematsu M, et al. Differential metabolomics reveals ophthalmic acid as an oxidative stress biomarker indicating hepatic glutathione consumption. J Biol Chem 2006;281:16768–76.
16. Soga T, Heiger DN. Amino acid analysis by capillary electrophoresis electrospray ionization mass spectrometry. Anal Chem 2000;72:1236–41.
17. Soga T, Ishikawa T, Igarashi S, Sugawara K, Kakazu Y, Tomita M. Analysis of nucleotides by pressure-assisted capillary electrophoresis-mass spectrometry using silanol mask technique. J Chromatogr A 2007;1159:125–33.
18. Smith CA, Want EJ, O'Maille G, Abagyan R, Siuzdak G. XCMS: processing mass spectrometry data for metabolite profiling using nonlinear peak alignment, matching, and identification. Anal Chem 2006;78:779–87.
19. Baran R, Kochi H, Saito N, et al. MathDAMP: a package for differential analysis of metabolite profiles. BMC Bioinformatics 2006;7:530.
20. Saeed AI, Sharov V, White J, et al. TM4: a free, open-source system for microarray data management and analysis. Biotechniques 2003;34:374–8.
21. Koukourakis MI, Pitiakoudis M, Giatromanolaki A, et al. Oxygen and glucose consumption in gastrointestinal adenocarcinomas: correlation with markers of hypoxia, acidity and anaerobic glycolysis. Cancer Sci 2006;97:1056–60.
22. Pedersen PL, Mathupala S, Rempel A, Geschwind JF, Ko YH. Mitochondrial bound type II hexokinase: a key player in the growth and survival of many cancers and an ideal prospect for therapeutic intervention. Biochim Biophys Acta 2002;1555:14–20.
23. Shakoori A, Ougolkov A, Yu ZW, et al. Deregulated GSK3b activity in colorectal cancer: its association with tumor cell survival and proliferation. Biochem Biophys Res Commun 2005;334:1365–73.
24. Koukourakis MI, Giatromanolaki A, Polychronidis A, et al. Endogenous markers of hypoxia/anaerobic metabolism and anemia in primary colorectal cancer. Cancer Sci 2006;97:582–8.
25. Mazzanti R, Solazzo M, Fantappie O, et al. Differential expression proteomics of human colon cancer. Am J Physiol Gastrointest Liver Physiol 2006;290:G1329–38.

26. Argilés JM, Azcón-Bieto J. The metabolic environment of cancer. Mol Cell Biochem 1988;81:3–17.
27. Pan JG, Mak TW. Metabolic targeting as an anticancer strategy: dawn of a new era? Sci STKE 2007;381:pe14.
28. Brahimi-Horn MC, Chiche J, Pouysségur J. Hypoxia signalling controls metabolic demand. Curr Opin Cell Biol 2007;19:223–9.
29. Lu J, Kunimoto S, Yamazaki Y, Kamiishi M, Esumi H. Kigamicin D, a novel anticancer agent based on a new anti-austerity strategy targeting cancer cells' tolerance to nutrient starvation. Cancer Sci 2004;95:547–52.
30. Wiesner RJ, Kreutzer U, Rosen P, Grieshaber MK. Subcellular distribution of malate-aspartate cycle intermediates during normoxia and anoxia in the heart. Biochim Biophys Acta 1988;936:114–23.
31. Kita K, Hirawake H, Miyadera H, Amino H, Takeo S. Role of complex II in anaerobic respiration of the parasite mitochondria from Ascaris suum and Plasmodium falciparum. Biochim Biophys Acta 2002;1553:123–39.
32. Ullmann R, Gross R, Simon J, Unden G, Kroger A. Transport of C4-dicarboxylates in Wolinella succinogenes. J Bacteriol 2000;182:5757–64.
33. Medina MA, Sánchez-Jiménez F, Márquez J, Rodríguez Quesada A, Núñez de Castro I. Relevance of glutamine metabolism to tumor cell growth. Mol Cell Biochem 1992;113:1–15.
34. Moreadith RW, Lehninger AL. The pathways of glutamate and glutamine oxidation by tumor cell mitochondria. Role of mitochondrial NAD(P)+-dependent malic enzyme. J Biol Chem 1984;259:6215–21.
35. Phang JM, Donald SP, Pandhare J, Liu Y. The metabolism of proline, a stress substrate, modulates carcinogenic pathways. Amino Acids 2008;35:681–90.
36. Droge W. Autophagy and aging-importance of amino acid levels. Mech Ageing Dev 2004;125:161–8.
37. Mizushima N, Klionsky DJ. Protein turnover via autophagy: implications for metabolism. Annu Rev Nutr 2007;27:19–40.
38. Sato K, Tsuchihara K, Fujii S, et al. Autophagy is activated in colorectal cancer cells and contributes to the tolerance to nutrient deprivation. Cancer Res 2007;67:9677–84.
39. Fujii S, Mitsunaga S, Yamazaki M, et al. Autophagy is activated in pancreatic cancer cells and correlates with poor patient outcome. Cancer Sci 2008;99:1813–9.
40. Chapman AG, Fall L, Atkinson DE. Adenylate energy charge in Escherichia coli during growth and starvation. J Bacteriol 1971;108:1072–86.
41. Buckstein MH, He J, Rubin H. Characterization of nucleotide pools as a function of physiological state in *Escherichia coli*. J Bacteriol 2008;190:718–26.
42. Hisanaga K, Onodera H, Kogure K. Changes in levels of purine and pyrimidine nucleotides during acute hypoxia and recovery in neonatal rat brain. J Neurochem 1986;47:1344–50.
43. Chapman AG, Atkinson DE. Stabilization of adenylate energy charge by the adenylate deaminase reaction. J Biol Chem 1973;248:8309–12.
44. Gatenby RA, Smallbone K, Maini PK, et al. Cellular adaptations to hypoxia and acidosis during somatic evolution of breast cancer. Br J Cancer 2007;97:646–53.